The influence of present-day regional surface mass balance uncertainties on the future evolution of the Antarctic Ice Sheet

Christian Wirths[1,2], Johannes C. R. Sutter[1,2], and Thomas F. Stocker[1,2]

[1]Climate and Environmental Physics, University of Bern
[2]Oeschger Centre for Climate Change Research, University of Bern

Correspondence: Christian Wirths (christian.wirths@unibe.ch)

Abstract. Rising global sea levels are one of many impacts, the current anthropogenic global warming poses to humanity. The Antarctic Ice Sheet (AIS) has the potential to contribute several meters of sea level rise over the next few centuries. To predict future sea level rise contributions from ice sheets, both global and regional climate model (RCM) outputs are used as forcing in ice sheet model simulations. While the impact of different global models on future projections is well-studied, the impact of

5   different regional models on the evolution of the AIS is not well-constrained. In our study, we investigated the impact of the choice of present-day reference RCM forcing on the evolution of the AIS. We used the Parallel Ice Sheet Model (PISM) to study the AIS in a constant forcing quasi-equilibrium state and under future projections, combining present-day RCM output with global climate model projections. Our study shows that the choice of RCM reference forcing results in uncertainties of future sea level rise predictions of 8.7 (7.3-9.5) cm in the year 2100 and 24.3 (16.3 - 46.5) cm in 2300 under the RCP8.5 scenario.

10   Those uncertainties are of the same order of magnitude as the choice of the underlying ice sheet model parameterization and global climate model. Additionally, our study shows that the choice of RCM reference affects the extent of grounding line retreat in West Antarctica in future projections and can result in the potential long-term collapse of the West Antarctic Ice Sheet in quasi-equilibrium simulations. Our study therefore highlights the importance, of a careful choice of RCM reference forcing for simulations of the AIS.

15 **1 Introduction**

Global sea level rise is one of many climate impacts due to anthropogenic global warming (IPCC, 2022). Until the end of this century model based estimates of global see level rise range from 0.44–0.76 m for SSP3-4.5 (IPCC, 2022) threatening flood prone areas populated by over 420 million people (Hooijer and Vernimmen, 2021). Besides ocean thermal expansion, the melting of the Greenland and Antarctic ice sheets is the largest current contributor to sea level rise (IPCC, 2022). Despite the

20 fact that the Antarctic ice sheet (AIS) is 7.8 (Morlighem et al., 2017, 2020) times larger than the Greenland ice sheet (GrIS), it currently contributes 3.6 ± 0.5 mm (Rignot et al., 2019) per decade to global sea level rise, which is a almost two times smaller contribution compared to the GrIS (WCRP Global Sea Level Budget Group, 2018). However observations show that the Antarctic melt contribution has been accelerating (Otosaka et al., 2023) and could become the largest contributor by the end of the century (Seroussi et al., 2020). The West Antarctic Ice Sheet (WAIS), which holds ice masses equivalent to ca. 3.3

25   m (Bamber et al., 2009) of sea level rise, might undergo a rapid melt in the coming century's due to its exposition to the so called marine ice sheet (MISI) (Schoof, 2007; Pattyn, 2018) and ice cliff instabilities (MICI) (DeConto and Pollard, 2016; Pattyn, 2018). Model based projections of Antarctic sea level contributions at the end of the century are associated with large uncertainties which can be reduced by careful calibration of the model involved (Bevan et al., 2023). Projections vary from -37 $\pm$ 34 mm to 96 $\pm$ 76 mm (Seroussi et al., 2020) for the RCP8.5 scenario. Those uncertainties have many reasons spanning

30   from largely unconstrained boundary conditions like basal friction (Bulthuis et al., 2019), ice shelf mass balance uncertainties arising from melt rate parameterizations and projected ocean temperature changes below the ice shelves and the evolution of the surface mass balance (SMB). The latter, estimates of Antarctica's SMB - the net accumulation rate of snow and ice on the surface of Antarctica - have been discussed in detail recently (Mottram et al., 2021). Direct observations of accumulation and surface melt are sparse, while SMB products from regional climate models have a large spread (ranging from 1961 $\pm$ 50 to

35   2519 $\pm$ 118 Gt yr^{-1} (Mottram et al., 2021)).

Uncertainties in Antarctica's current SMB affect prognostic or paleo ice sheet model (ISM) simulations which often use output from RCMs as a reference baseline forcing upon which climate anomalies are then added. The SMB data from RCMs are used to establish the present-day reference forcing and projections or reconstructions of future and past Antarctic climate

40   change are added to this forcing via anomalies (usually computed against the pre-industrial or historical mean of the respective climate model) (Sutter et al., 2019; Nowicki et al., 2020; Seroussi et al., 2020; Sutter et al., 2021; Reese et al., 2022). There is a variety of different RCM SMB-products available for ice-sheet modeling, from which a selection is presented in Fig. 1. Those SMB fields do not only differ in the total SMB they produce for Antarctica but also in the spatial distribution (Mottram et al., 2021). However, many modelling studies utilize data from the RACMO model (Seroussi et al., 2020). This model is designed

45   to simulate polar regions since it accounts for many relevant processes as snow drifting, melt, refreezing and percolation (van Wessem et al., 2018). However, there is not a specific reason to exclusively use one model. A recent study by Li et al. (2023) suggests that the difference in SMB from different global models can have a substantial impact on the equilibrium state of the AIS. This has also been shown in the results of Seroussi et al. (2020).

50   In this study we investigate the response of the AIS to different forcings derived from a range of RCMs adressing the following questions: i) How does the choice of reference SMB and surface air temperature forcing affect the quasi-equilibrium state of the AIS? ii) How does this choice affect the evolution of the AIS under different climate scenarios? iii) Does this choice have an impact the projected stability of marine ice sheets?

55   In the upcoming sections, we introduce the RCM products utilized in our study and describe our simulation setup for the AIS. We then present the results from our long-term equilibrium simulations and future projections. Finally, we discuss the implications of the choice of RCM product on the evolution and stability of the AIS.
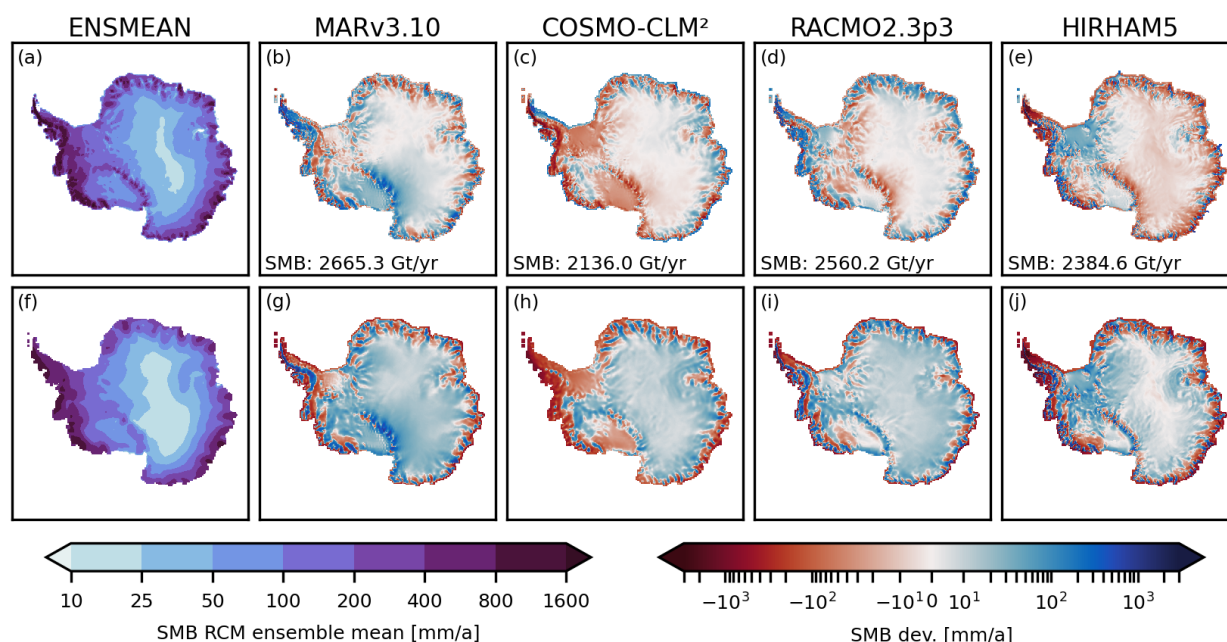
Figure 1. Surface mass balance (SMB) of the (a) multi-RCM mean and anomalies of the (b) MARv3.10 (Kittel et al., 2020), (c) COSMO-CLM^2 (Souverijns et al., 2019), (d) RACMO2.3p3 (van Dalum et al., 2021), and (e) HIRHAM5 (Hansen et al., 2022) regional climate model from this mean. Further the anomalies of the ERA-Interim dataset (Dee et al., 2011) to the multi RCM mean (f), (g) MARv3.10 (h) COSMO-CLM^2 (i) RACMO2.3p3 (j) HIRHAM5 RCM. The surface mass balance was averaged over the period from 1987-2016.

2 Methods

To address these questions posed above, we consider two different model setups. In the first we assess the equilibrium ice sheet response for a range of reference present-day baseline climate forcings. In the second we investigate the imprint of the present-day baseline climatology on ice sheet model projections under a set of CMIP5 scenarios. In the following we will briefly describe the ice sheet model setup (spinup, present-day equilibrium and prognostic simulations) and introduce the applied regional climate model forcing which will be used as a baseline climatology in all experiments.

2.1 SMB forcings

There is a considerable spread of model-based present-day surface mass balance (SMB) estimates (c.f. Fig. 1). To assess the equilibrium and transient ice sheet response to this spread we force the ISM with surface air temperature and surface mass balance derived from four regional climate models (RCMs): MARv3.10 (Kittel et al., 2020), COSMO-CLM^2 (Souverijns et al., 2019), RACMO2.3p3 (van Dalum et al., 2021) and HIRHAM5 (Hansen et al., 2022). A general overview of those models as well as the applied forcings, parametrizations, and submodules are provided in Table 1. An additional SMB comparison for

	MARv3.10	COSMO-CLM2	RACMO2.3p3	HIRHAM5
Resolution	35km	25km	27km	12/50km
	24 layers	40 layers	40 layers	31 layers
Surface scheme	SISVAT	CLM	internal snow model	-
	based on (Ridder and Gallée, 1998)	(Oleson et al., 2013)	(Ettema et al., 2010)	
Boundary conditions	ERA-Interim	ERA-Interim	ERA-Interim	ERA-Interim
Boundary interval	6h	6h	6h	6h
Nudging	Yes	Yes	Yes	No
Direct SMB	Yes	No	Yes	No

Table 1. Summary of the regional climate model configuration for MARv3.10 (Kittel et al., 2020), COSMO-CLM2 (Souverijns et al., 2019), RACMO2.3p3 (van Dalum et al., 2021), and HIRHAM5 (Hansen et al., 2021).

70 the individual IMBIE drainage basin can be found in Fig. A1. All four models, were forced with the ERA-Interim reanalysis (Dee et al., 2011) at the domain boundaries, with the MARv3.10, RACMO2.3p3 and COSMO-CLM^2 model being nudged into the domain by applying upper air relaxation (van de Berg and Medley, 2016). In contrast HIRHAM evolved freely and was only forced at the boundary of the domain (Mottram et al., 2021). RACMO and MAR have optimized subsurface snow and ice schemes to take meltwater, refreezing and retention into account. Additionally, RACMO accounts for wind driven erosion and

75 sublimation of blown-off snow (Lenaerts et al., 2012). A more detailed discussion and comparison of the applied RCMs can be found in Mottram et al. (2021).

To conduct our study, we obtained the SMB-forcing either directly from the model output (MAR and RACMO) or calculated SMB as described by Mottram et al. (2021) from precipitation, evaporation, and sublimation. Please note that for COSMO the

80 difference between precipitation and sublimation and for HIRHAM the difference between precipitation, sublimation, and evaporation is used to calculate the SMB. We then calculated the climatic mean of the SMB and surface temperature for the common period from 1987 to 2016 and bi-linearly regridded the data to the PISM domain at 8km resolution. The SMB ensemble mean of those RCMs togeher with the deviation of the individual RCM SMBs from this mean and the total mass balance are shown in Fig. 1. Please note that due to the regridding as well as the chosen ice mask we expect the total SBM to

85 differ slightly from values of other publications (Hansen et al., 2022).

2.2 Ice-sheet model set up

To simulate the response of the Antarctic Ice sheet, we employ the thermodynamially-coupled Parallel Ice Sheet Model (PISM) (Bueler and Brown, 2009; Winkelmann et al., 2011). We employ PISM in a hybrid mode using the shallow ice (SIA) and shallow shelf approximation (SSA) to efficiently simulate the slow ice domes as well as the fast ice-streams of outlet glaciers

and shelf's. The stress at which the ice starts to slide by deformation of the till layer, also called yield stress

$$\tau_C = c_0 + tan(\phi)\, N_{till} \tag{1}$$

is calculated following the Mohr-Coulomb law (Cuffey and Paterson, 2010), with the till friction angle ϕ, the effective till pressure N_{till} and the "till cohesion" c_0. The till friction angle depends on the bed topography and is linearly interpolated between ϕ_{min} and ϕ_{max} for bed elevations between b_{min} and b_{max} with the gradient $M = (\phi_{max} - \phi_{min})/(b_{max} - b_{min})$ by

$$\phi(x,y) = \begin{cases} \phi_{min}, & b(x,y) \leq b_{min}, \\ \phi_{min} + (b(x,y) - b_{min})M, & b_{min} < b(x,y) < b_{max}, \\ \phi_{max}, & b_{max} \leq b(x,y) \end{cases} \tag{2}$$

(Aschwanden et al., 2013; Winkelmann et al., 2011; Martin et al., 2011). Sub-shelf melt and refreezing at the ice ocean interface is calculated using PICO (Reese et al., 2018), an ocean box model which mimics the overturning circulation in the cavities below the ice shelf.

In this study we consider two model set ups, performing long term (30 ka) present-day equilibrium simulations with a constant present-day forcing and centennial projections until the year 2300 applying climate anomalies from HadGEM-ES2 (Jones et al., 2018) for the RCP2.6, RCP4.5 and RCP8.5 scenario. In both cases, the model is initialized from the BEDMACHINE (Morlighem et al., 2020) bedrock topography and ice thickness. Additionally, geothermal heat-flux data by Shapiro and Ritzwoller (2004), is applied. As an initial step we perform a 200 ka thermal spinup during which the ice surface elevation is fixed and the ice sheet is forced with surface air temperature from RACMO2.3p3 (van Dalum et al., 2021) and geothermal heat flux from Shapiro and Ritzwoller (2004). Following this spinup procedure the present-day equilibrium and prognostic simulations are branched off.

2.2.1 Long term present-day equilibrium simulations

To explore the equilibrium response of the Antarctic Ice Sheet to the four RCM forcings considered here, we perform a set of long term present-day equilibrium simulations. Therefore, we restart the model from the thermal spinup applying constant SMB and temperature forcing fields from the individual RCMs and let the model freely evolve for 30 000 years (c.f. Fig. 2) on 16 km resolution. To compute basal melting underneath the ice shelves, we additionally force the model with ocean temperature and salinity from the Word ocean database (WOA) (Boyer et al., 2018). For every RCM- forcing we employ 14 simulations with different combinations of the shallow ice approximation enhancement factor sia_e, the pseudo plastic parameter pQ (used in the pseudo plastic sliding law), the minimum till friction angle ϕ_{min} (the angle we assume for marine basins below -700m as in (Albrecht et al., 2020)), and the heat conductivity at the ice-ocean interface γ. For detailed list of the parameters see Table 2. The parameter combinations were selected based on the model skill to reproduce the observed present-day ice thickness, surface velocities and grounding line (Morlighem et al., 2020). An additional constrained was the

sea-level equivalent ice volume after 15 000 years under constant RACMO2.3p3 forcing. Here we penalized deviations from
120   present-day estimates of Antarctica's current ice volume. The comparison and scoring was performed following the scoring
method by Albrecht et al. (2020). An additional and more rigid selection of parameter sets was performed by only choosing
parameter combinations which ensure long term stability of WAIS (central WAIS being glacierized for more than 100 000
years) under the RACMO2.3p3 forcing. This is a conservative assumption as for example parts of the WAIS already undergo
substantial grounding line retreat which could lead to a long term collapse of the WAIS (Reese et al., 2022). The chosen spinup
125   method and parameter selection process is not necessarily the most rigid in terms of producing a good match with present-day
ice sheet observations. A much better fit can be achieved via inversion or iterative optimization of e.g. a sliding parameter
as e.g. done in (Pollard and DeConto, 2012; Li et al., 2023). The latter method can either be applied for only one forcing
or for all forcings individually. Nevertheless, both approaches have drawbacks when applied to our context. On the one hand,
individually applying the inversion or iterative optimization technique to each forcing field would select basal sliding properties
130   for each forcing field in a manner that converges toward a state closest to observational data, thereby concealing disparities
inherent in the forcing fields within the basal sliding component. This evidently annihilates the core objective of this study,
which centers around discerning the distinct influences exerted by individual forcing fields on the ice sheet.

Conversely, fine-tuning the basal sliding coefficients exclusively to a specific forcing field carries the risk of overly tailoring
the model to that particular forcing field, potentially leading to overfitting. Such meticulously calibrated basal sliding conditions
135   might not be suitable for other forcing fields, potentially resulting in unrealistic ice sheet dynamics when subjected to those
fields. Generally, this trade-off necessitates consideration for each instance of tuning and parameter selection. Nonetheless, our
approach employs consistent basal sliding conditions across all forcing fields, while also calibrating for overarching global
parameters. This not only accelerates and renders the computation more cost-effective, but also mitigates the possibility of
introducing artifacts by excessively tuning the model to any single forcing field.

2.2.2   Centennial projections of Antarctic Ice Sheet evolution.

In order to assess the impact of present-day baseline climate forcings on centennial sea level projections we perform simulations
until the year 2300 applying transient annual climate anomalies derived from HadGem2-ES (Jones et al., 2018) RCP-scenarios.
We restart the model after the thermal spinup to perform an 1860-2005 C.E. historical spinup (c.f. Fig. 2) on 8 km resolution.
For the historical spinup and projections, transient annual mean surface air temperature and SMB anomalies from HadGEM2-
145   ES (Jones et al., 2018) are added to the respective present-day RCM climatology to produce the climate forcing until the year
2300. Likewise ocean temperature and salinity anomalies are added to the WOA ocean forcing. After the historical spinup we
branch the individual simulations into four different forcing scenarios and let the model evolve until the year 2300. The four
different branches consist of a control run, which applies constant 2005 climate conditions, as well as RCP2.6, RCP4.5, and
RCP8.5 scenarios which use the anomalies from the HadGEM2-ES model. Similar to the present-day equilibrium runs we
150   choose an ensemble of different parameter configurations but without explicitly excluding configurations without long term
stability. The complete list of selected parameter configurations is provided in Table 2. Please note that since the model spinup
we chose here is relatively simple compared to e.g. inversion or a full glacial interglacial paleo-spinup model biases are to
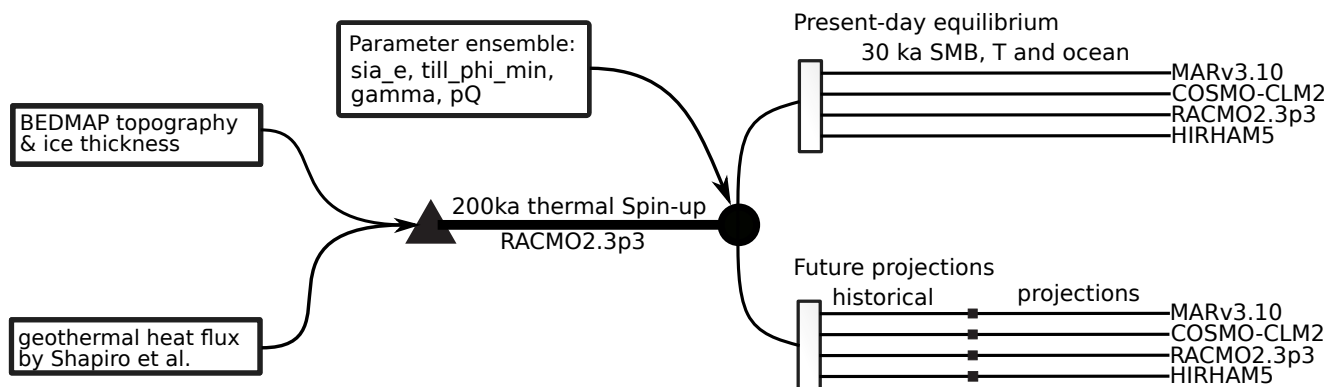
Figure 2. Illustration of the present-day equilibrium simulation and future projections setup: First the model is initialized from present-day ice sheet observations. Then a 200 ka thermal spinup is performed. For the present-day equilibrium 14 individual simulations are performed for each of the four constant RCM forcing fields and allowing the model to freely evolve for 30 000 years. For the future projections, starting after the thermal spinup, an historical spinup, using HadGem2-ES (Jones et al., 2018) anomalies, is performed for every RCM forcing set. Then, we run 10 individual simulations for every combination of the RCM forcing fields with the four climate pathways (2005 control, RCP2.6, RCP4.5, RCP8.5).

Setup	sia_e	pQ	$\gamma \, [\times 10^{-5}]$	$\phi_{till\,min}$
PD-equilibrium	1.00, 1.25, 1.50	0.60, 0.75, 0.80	2.0, 2.5, 3.0	2, 4
Future projections	1.00, 1.25, 1.50	0.75, 0.8	2.0, 2.5, 4.0	4, 6

Table 2. Chosen parameter space for the shallow ice approximation enhancement factor sia_e, the pseudoplastic pQ factor, the heat conductivity at the ice ocean interface γ, and the minimum till friction angle $\phi_{till\,min}$ for the present-day pseudo equilibrium runs as well as the future projections.

be expected. In consequence, the initial ice sheet configuration lacks a realistic thermal state and as we do not use iterative optimization (see above) model deviations with respect to ice thickness can be rather large. However, as these kinds of simple

155   spinup routines have often been used in the past we considered this to be a valid approach to assess the impact of present-day climate forcing uncertainties on future and equilibrium ice sheet evolution in typical model setups. Therefore, this setup is not designed to give robust projections on future Antarctic sea level contributions but rather serves to estimate uncertainties arising from different RCM forcing fields.

3 Results

160 In this section we present the evolution of ice volume and area under constant present-day forcing and centennial future projections. We further discuss the imprint of SMB forcing differences on ice thickness and grounding line position at the end of the respective simulations.

3.1 Impact of RCM forcing on the present-day quasi-equilibrium state
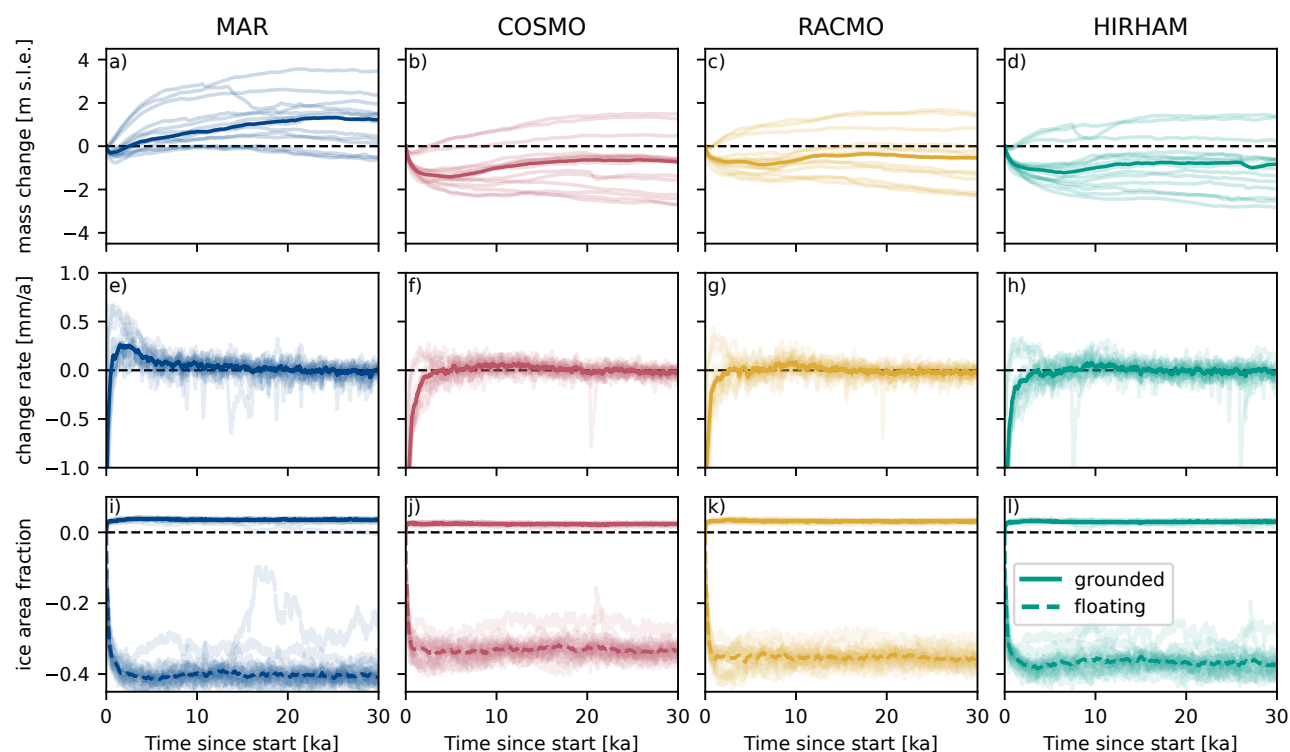

Figure 3. Time series of the total ice mass change (a-d), the annual rate of change (e-h), and the fraction of grounded (solid line) and floating (dashed line) ice area (i-l) relative to observations for the four different RCM forcing fields. Bold line shows ensemble median while shaded lines indicate the individual ensemble members.

3.1.1 Impact of RCM forcing on global ice mass and extend

165 Starting from the present-day observations the total ice volume (c.f. Fig. 3 a-d) undergoes an initialization shock after which the rate of change (c.f. Fig. 3 e-h) converges towards zero. After 30 000 years of simulation the median change in ice volume is negative (i.e. ice loss) for three (COSMO: -0.74 m, RACMO: -0.53 m, HIRHAM: -0.84 m) out of the four models. The simulations which apply the RACMO forcing show the least change in ice volume. In contrast, ice sheet simulations

using the MAR forcing exhibit an increase in SLE volume compared to present-day observations by 1.21 meters. Although
170 the annual rate of mass change converges towards zero, the ensemble spread indicates that the ice sheets is still undergoing
small fluctuations in ice sheet mass between -0.16 mm/a and 0.14 mm/a (current AIS sea level contribution is ≈ 0.3 mm per
year (Shepherd et al., 2018)). The initialization shock observed in the ice volume change is also reflected in the respective
ice area change of floating and grounded ice. For all models an increase in the grounded ice area with a coinciding decrease
in the ice shelf area is observable - a result of an advancing grounding line in the Filchner-Ronne ice shelf (c.f. Fig. 4). The
175 median decrease in ice shelf area varies between -41% and -34% with MAR showing the largest and COSMO the smallest
decrease (this might be due to the weak SMB over ice shelves in COSMO compared to the other RCMs). The main cause of
this decrease is grounding line advance with MAR showing the largest (3.6%) and COSMO the smallest (2.4%) corresponding
growth in grounded ice area. The time series presenting the impact of the ensemble mean RCM forcing can be found in Fig. B3.

3.1.2 Impact of RCM forcing on regional ice cover

We now turn to regional characteristics of the simulated ice sheet. When we compare the ice thickness between present-day
observations and our simulations after 30 000 years a distinct pattern arises which is independent of ensemble member and
RCM forcing field (c.f. Fig. B1). All our simulations show a strong negative ice thickness anomaly in the WAIS which is mainly
driven by ice sheet model parameterisation. Additionally, all realizations show ice loss at the EAIS margins with substantial
185 coastal ice sheet thinning in George V and Wilkes Land. In contrast, larger ice thickness is simulated in Oates Land along the
Transantarctic mountains and also on the Antarctic Peninsula, the Ellsworth and Scott Mountains as well as at the Shackleton
range. The inter-model differences caused by the different RCM-forcings (mainly the impact of SMB forcing differences) are
around four times smaller compared to overall model bias (effect of ice sheet model spinup and parameter choices).

190   Therefore, we explicitly illustrate the differences between the individual RCM forcing sets in Fig. 4. Panel (a-d) depicts the
ice thickness differences Δh for each individual RCM forcing set from the common mean of all four forcing sets. At every
grid cell (i,j) and for a given $RCM \in \{MAR, COSMO, RACMO, HIRHAM\}$, Δh is given as:

$$\Delta h_{i,j}^{RCM} = h_{i,j}^{RCM} - \frac{h_{i,j}^{MAR} + h_{i,j}^{COSMO} + h_{i,j}^{RACMO} + h_{i,j}^{HIRHAM}}{4}. \tag{3}$$

Due to its overall higher SMB, the simulations forced with the MAR data show positive Δh, except for small negative
195 Δh values at the Princess Ranghild Coast and the George V Land. Additionally, simulations forced with SMB and surface
temperature from COSMO, RACMO, and HIRHAM show diverging Δh patterns between East and West Antarctica which
generally agree with the differences in their undelining SMB forcing. For all four forcing fields we illustrate the regions of
highest ensemble variability in ice thickness (Fig. 4 (e-f)). Wilkes and Aurora Subglacial Basins are the regions of highest
ensemble variability. Additionally, the Shackleton Range shows large ice thickness variability across all four forcing fields.
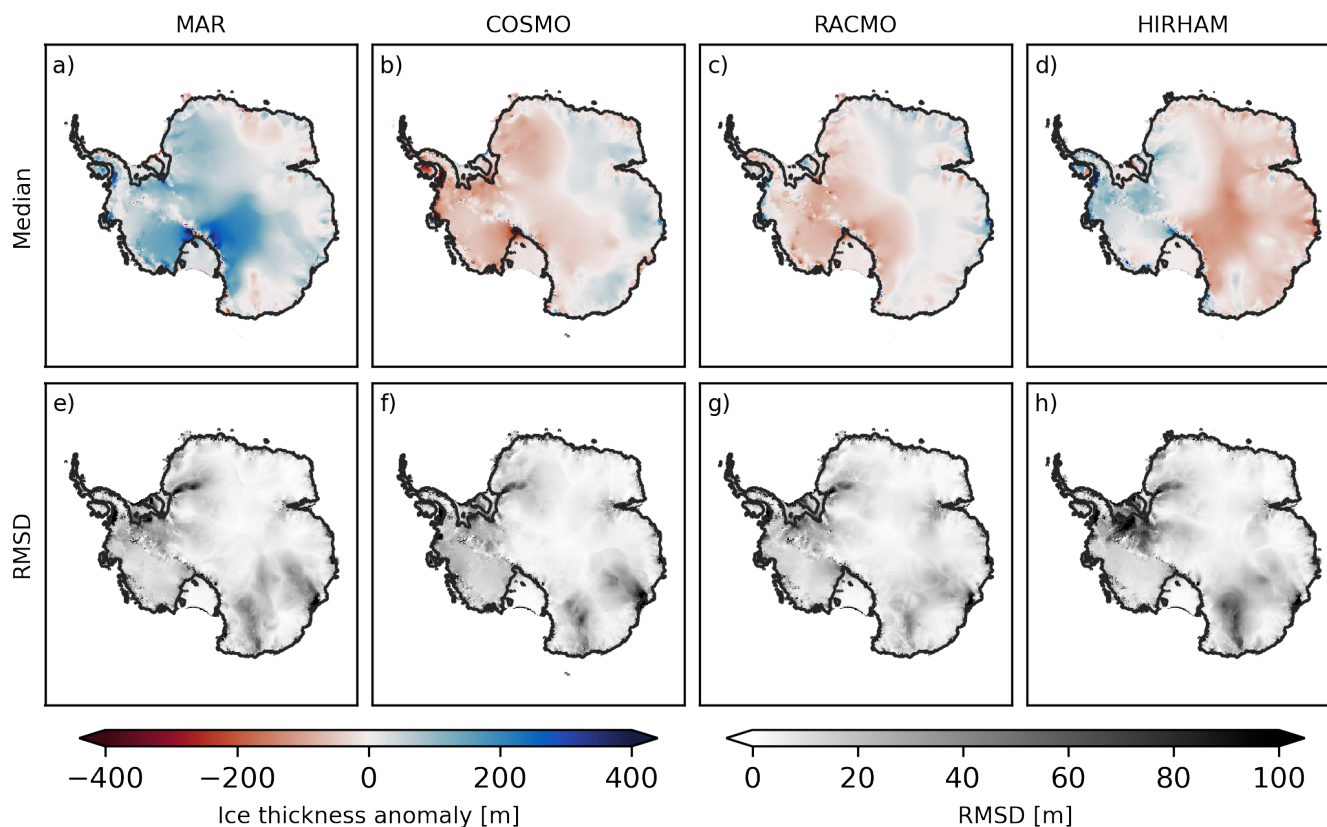
Figure 4. Ice thickness anomalies Δh from common mean (a-d), position of the simulated (purple) and observed (grey) grounding line for the present-day equilibrium simulations. Root mean square deviation (RMSD) of the individual ensemble members from the median (e-h). The difference between the common mean and the result of the forcing ensemble mean are illustrated in Fig. B4.

200 The HIRHAM forcing field exhibits high variability in Ellsworth Land.

3.1.3 Amplification of ISM uncertainties due to RCM selection

In order to illustrate differences in individual model runs and their evolution under constant present-day climate conditions, we illustrate the change in ice volume and ice thickness differences at the end of the simulation (after 30 ka) for two individual

205 parameter sets in Fig. 5. While parameter-set AX (c.f. Tab. C1) (panel a-e) reaches a quasi-equilibrium state relatively fast, parameter-set AY (panel f-j) exhibits a dynamical reorganization of WAIS evolution midway of the simulation. For the first 10 kyrs simulations forced by all RCMs quickly grow in ice mass. However, after 12 kyrs, a collapse of the WAIS leads to a ice volume loss equivalent of 1m s.l.e. in the simulation forced by MAR, which showed the strongest increase in ice mass in the beginning due to its high SMB. In addition, one has to note that the ice loss in WAIS is partially compensated for by a still
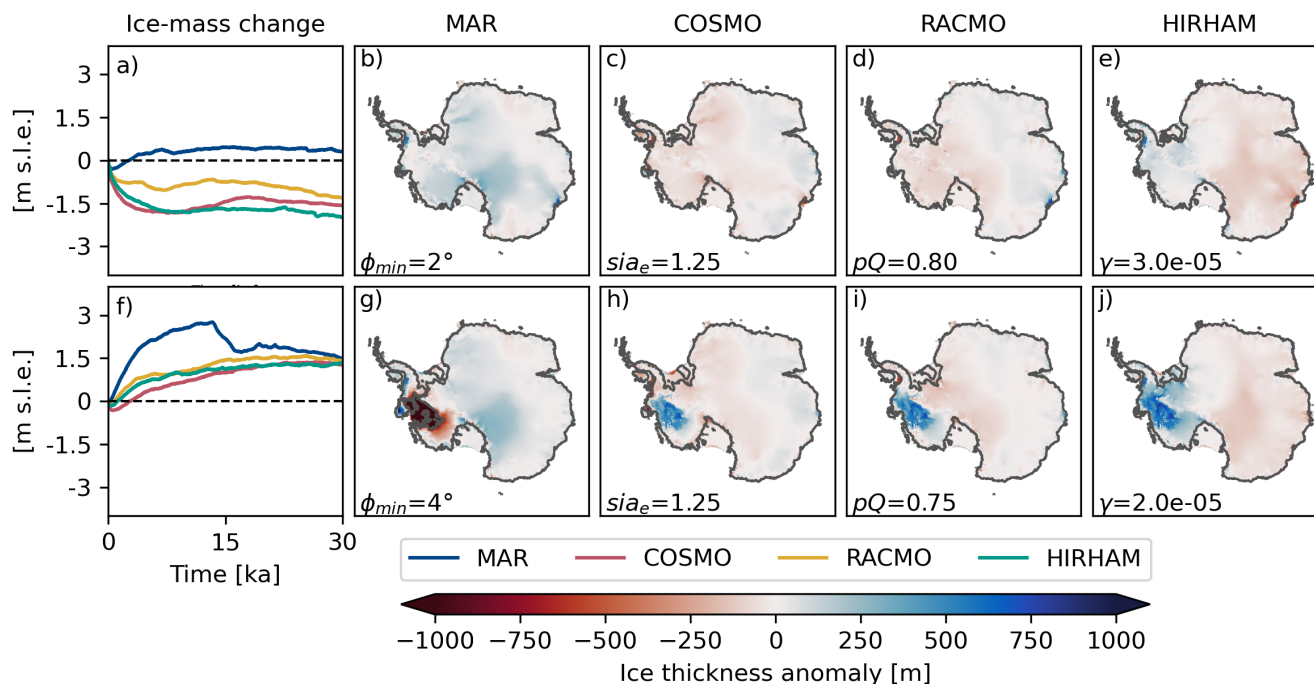
Figure 5. Evolution of the sea level change relevant ice masses (a,f) over the simulation period and ice thickness differences from the common mean as well as grounding line position (grey line) at the end of the simulation (b-e, g-j). Panel a-e show the results of the simulation with $\phi_{min} = 2°, sia_e = 1.25, pQ = 0.8, \gamma = 3.0 \times 10^{-5}$. Panel f-j show the results the simulation with $\phi_{min} = 4°, sia_e = 1.25, pQ = 0.75, \gamma = 2.0 \times 10^{-5}$. Please be aware of the changed color-scale w.r.t. Fig. 4.

growing ice sheet in Central and East Antarctica which combines together to the observed 1m s.l.e ice volume loss. Simulations forced by the other three RCMs in contrast steadily continue to grow and reach a quasi equilibrium at a similar state of ice mass change but with a present-day WAIS configuration. Similar model ensemble responses are produced if we loosen our restriction for stability under RACMO forcing, we defined in Section 2.2.1, from 100 kyrs down to 15 kyrs. Fig. C1 shows a selection from those simulations illustrating how the relatively small differences in SMB forcing can lead to large differences in the simulation outcome. For parameter-set CX (c.f. Tab. C1) (panel a-e) all models seem to smoothly approach a quasi equilibrium until a WAIS collapse after ca. 28ka occurs in the COSMO forced simulation. Simulations with parameter-set CY show a collapse for WAIS within the first 7 kyrs for MAR and COSMO forcing and a WAIS collapse around 22 kyrs for the HIRHAM forcing. Parameter-set CZ results in a WAIS collapse st 15 kyrs when forced by COSMO and at 23 kyrs when forced with RACMO.

3.2 Projections of present-day RCM imprint on centennial Antarctic Ice Sheet evolution

To investigate the effect of differences in the underlying RCM baseline data in a changing climatic environment we simulated the historical period from 1860 to 2005 and following the RCP2.6, RCP4.5, and RCP8.5 scenario until 2300 on a 8 km grid
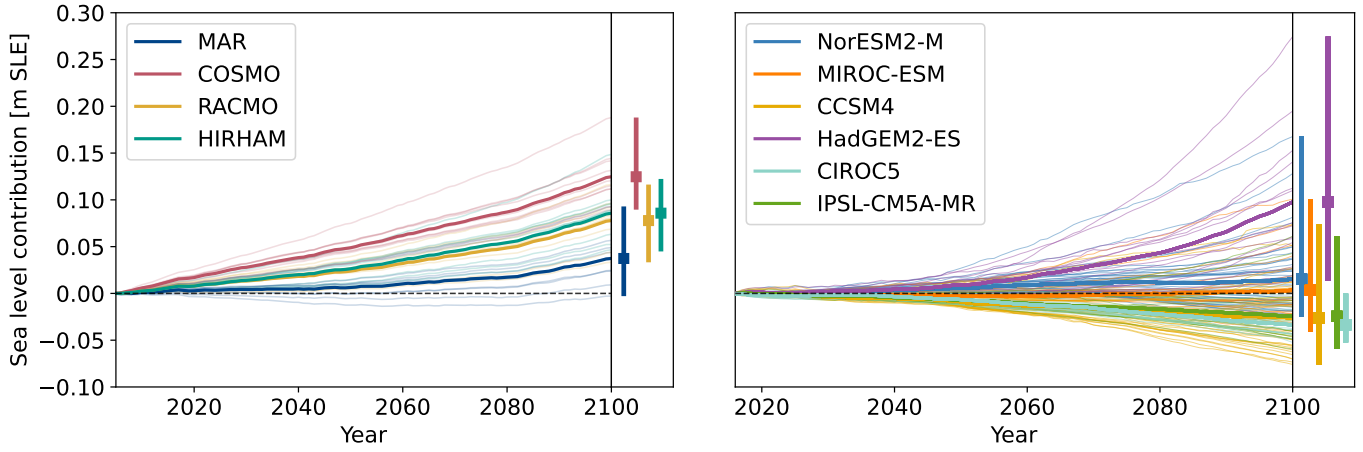
11

Figure 6. Antactic sea level rise contribution for the RCP8.5 scenario with different RCM present-day fields (a) as well as from ISMIP6 (Seroussi et al., 2020) (b) until the year 2100. Thin lines show individual simulations, bold lines the mean state for the different models. Note that in our study, GCM anomalies from HadGEM2-ES (Jones et al., 2018) were used together with RCM forcing fields.

resolution. The evolution of the total ice volume as well as grounded and floating ice area is shown in Fig. D1 and discussed in detail in the Appendix.

225

3.2.1 Imprint of RCM present-day forcing on sea level rise projections

In the following we show the uncertainties in sea-level rise projections which arise from the choice of RCM baseline data. Figure 6 illustrates the sea level rise contribution of the individual simulations until the year 2100 in the RCP8.5 scenario contrasted with the results from Seroussi et al. (2020). We estimate the maxmimum difference in sea level rise contribution

230 between simulations with different RCM reference forcings. Therefore we calculate for every member (par) of the parameter ensemble the maximum sea level contribution difference

$$\Delta slr_{par}^{max} = \max_{\mu,\nu \in \Omega} (slr_{par}^{\mu} - slr_{par}^{\nu}). \tag{4}$$

Here, $\Omega = \{MAR, COSMO, RACMO, HIRHAM\}$ denotes the list of potential RCM reference forcing. We then calculate the ensemble mean of Δslr_{par}^{max} (minimum and maximum are indicated in the brackets): Under the assumption of no

235 difference in the year 2005, Δslr^{max} in the year 2100 is 8.7 (7.3 - 9.5) cm for the RCP 8.5, 8.6 (8.0 - 9.8) cm for RCP4.5 and 8.6 (7.4 - 10.0) cm for RCP2.6. The numbers in the brackets indicate the range from minimum to maximum difference. Until the year 2300 those differences increase to 24.3 (16.3 - 46.5) cm for RCP8.5, 24.9 (21.9 - 28.3) cm for RCP4.5 and 23.3 (21.1 - 26.8) cm for RCP2.6.
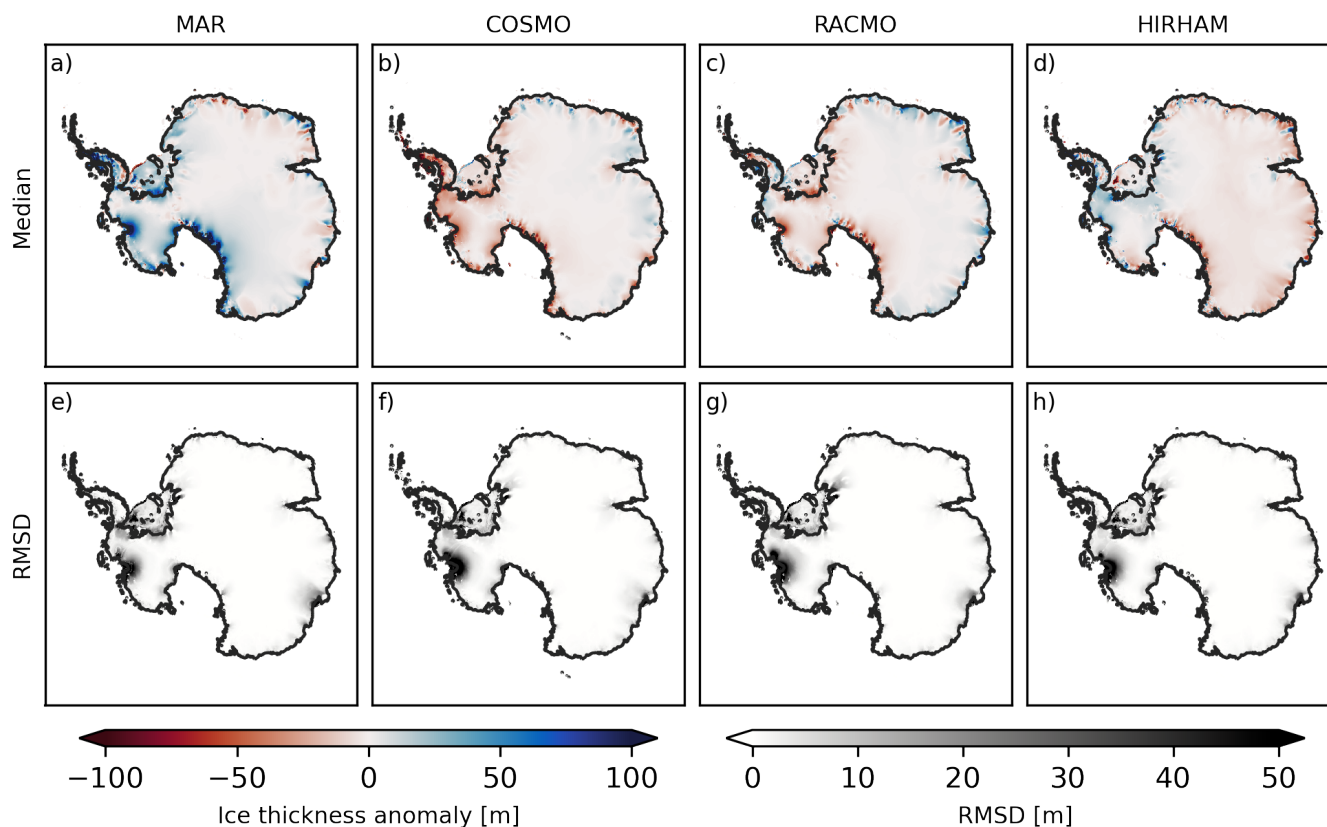
Figure 7. Ice thickness anomalies from common mean (a-d), position of the simulated (purple) and observed (grey) grounding line for the RCP8.5 future projection. Root mean square deviation (RMSD) of the individual ensemble members from the median (e-h). Please be aware that the used color-scale in this section is smaller than in the previous sections.

240   Furthermore, it is worth noting that the variations in sea-level rise contributions account for only 62% (in 2100) and 56% (in 2300) of the total integrated Surface Mass Balance (SMB) difference (The accumulated SMB differences is 14.0 cm and 43.4 cm SLE). However, it is important to consider that a large portion (ca. 150 Gt/year) of accumulation occurs over the ice shelves, which have a neutral effect on sea-level rise. When we account for this factor, we find that the difference in simulated sea-level rise contribution constitutes approximately 86% and 78% of the accumulated SMB The accumulated SMB differences is 10.1

245   cm and 31.3 cm SLE).

3.2.2 Impact of reference RCM on regional ice thickness

The spatial distribution of ice mass and area loss shown in Fig. 7 shows Δh and the simulated grounding line position at the year 2300 in the RCP8.5 scenario. The RCP2.6 and RCP4.5 scenarios are shown in Fig. D2 and Fig. D3. In all three sce-

250 narios a similar ice sheet response is simulated: Simulations forced with MAR generally show higher Δh especially along the Transantarctic mountains and in the Filchner ice shelf. In contrast, simulations forced by COSMO mainly depict negative Δh. Simulations forced by RACMO or HIRHAM show a general diverging pattern with mostly positive Δh over WAIS for HIRHAM and negative for RACMO. In East Antarctica the opposite is observable with positive Δh in simulations forced by RACMO and negative Δh for HIRHAM. Although the overall patterns of ice thickness changes are rather similar, for the

255 RCP4.5 and RCP8.5 scenario, major differences in ice thickness are observable at Thwaites glacier, with positive anomalies in MAR and HIRHAM and negative anomalies in COSMO and RACMO.

3.2.3 Ensemble sensitivity to reference RCM forcing

The sensitivity of Δh to ice sheet model parameters under a single RCM baseline reference forcing is shown by the root-

260 mean-square-deviation depicted in Figs. 7, D2 and D3. This allows the identification of regions where the chosen ice sheet model parametrization has a high impact on simulated ice thickness differences. For the RCP2.6 and RCP4.5 (see Figs. D2 and D3) emission scenario the largest parameter sensitivity can be observed at the Filchner-Ronne ice shelf and Totten Glacier. Additionally, slightly weaker sensitivity can be observed at Thwaites and Pine Island glacier. Simulations performed using the RACMO forcing also exhibit stronger parameter sensitivity at Slessor Glacier. For the RCP8.5 scenario (Fig. 7), Thwaites and

265 Pine Island Glacier exhibit the strongest parameter sensitivity. Still present but smaller in spatial extend is the region of high sensitivity at Totten Glacier. Compared to the RCP2.6 and RCP4.5 scenario the parameter sensitivity at the Filchner-Ronne ice shelf is reduced. Surprisingly, a large Δh does not necessarily also imply a large parameter-sensitivity. The Transantartic mountain range for example shows high absolute Δh values between different baseline models while the parameter sensitivity is particularly small.

270

3.2.4 Grounding line sensitivity to RCM baseline forcing

The regional impact (Amundsen Sea sector) of the applied forcings and parameter configuration are illustrated in Fig. 8. In the RCP2.6 scenario changes of grounding line positions with respect to the observed grounding line and the spread due to the RCM baseline forcings are rather small. However, simulations using the COSMO forcing differ either at Ellsworth land or at

275 the Pine Island glacier outlet. In the RCP4.5 scenario, the simulated grounding line deviation due to the different RCM-baseline forcing is more pronounced. Interestingly, some ice sheet model realisations (parameter combinations) suggest a significant grounding line advance for the RACMO baseline forcing while the three other RCM-cases suggest grounding line retreat (see Fig. 8 d). While differences in the grounding line position between the RCP2.6 and RCP4.5 scenarios are rather small, they are significantly bigger in the RCP8.5 scenario, where we can observe a larger retreat of the grounding line compared to present-

280 day locations and a large spread between the forcings as well as the respective parameter configurations. This shows that the choice of RCM baseline scenario will significantly affect the onset and pacing of a marine ice sheet instability in the Amundsen
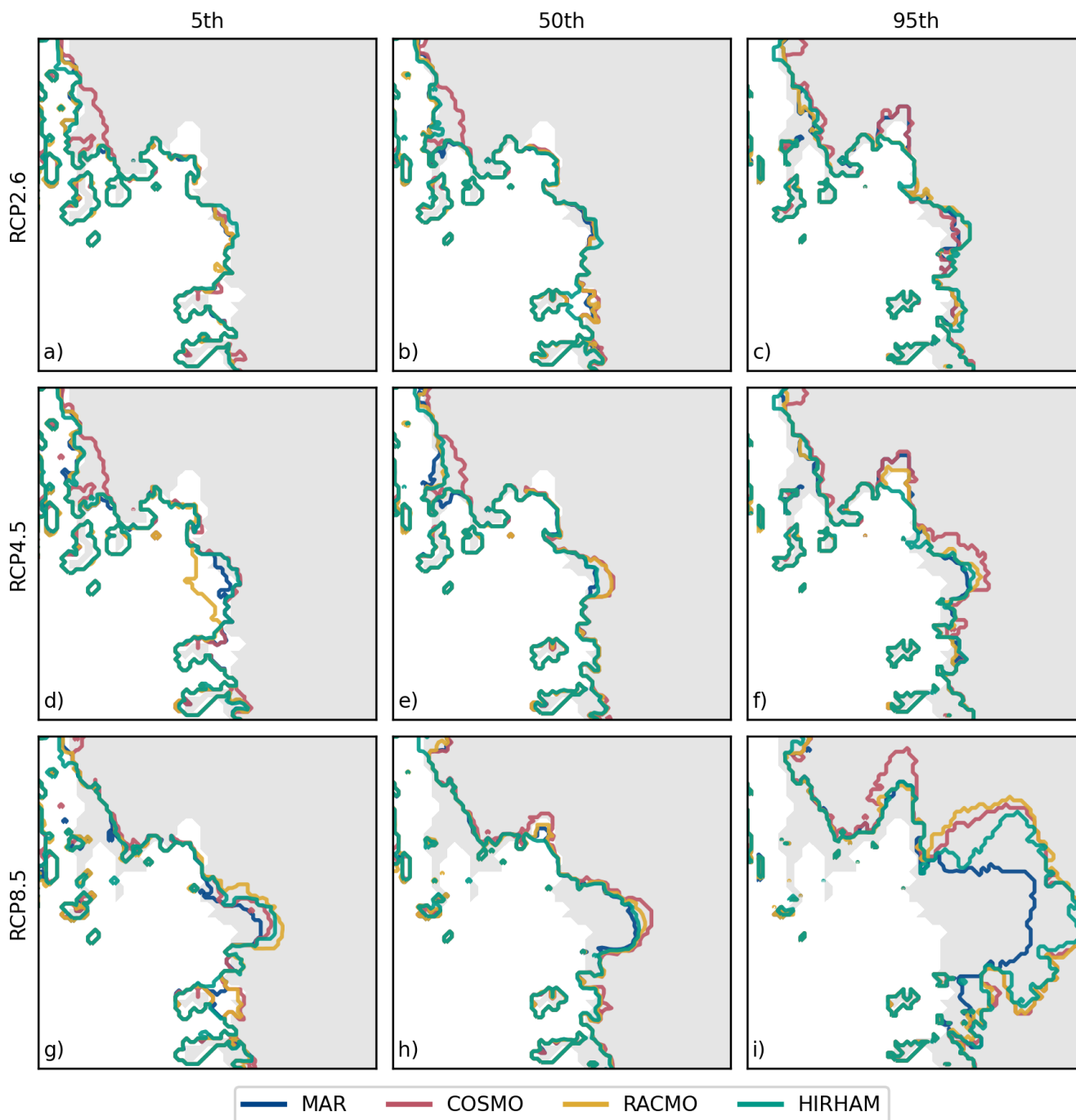
Figure 8. 5th, 50th and 95th percentile of grounding line position at the year 2300 for siumaltions using the four RCM forcing sets in the RCP2.6 (a-c), RCP4.5 (d-f) and RCP8.5 (g-i) scenario at Thwaites and Pine Island Glacier. Grey shaded area indicate observed present-day grounded ice extend.
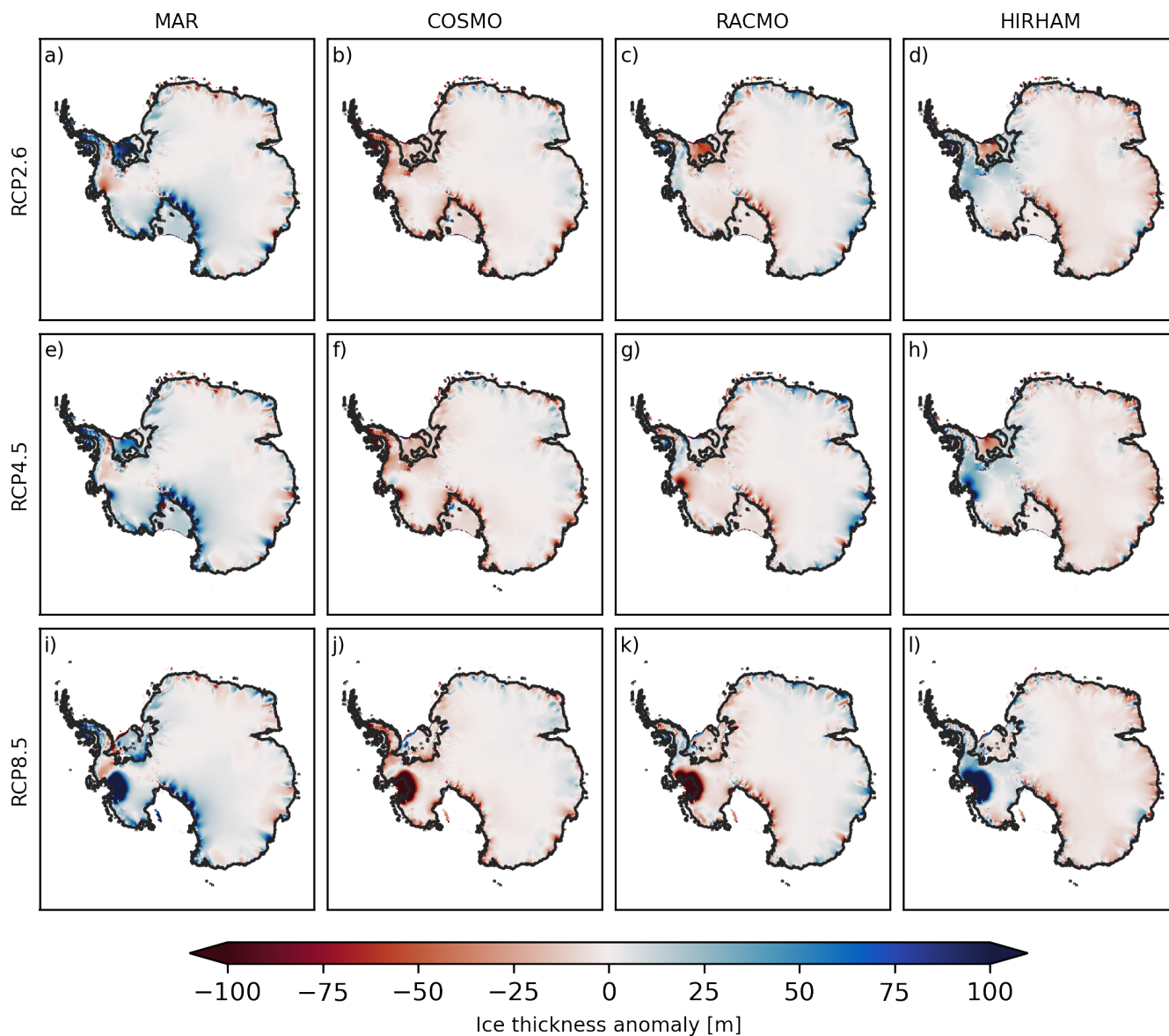
Figure 9. Ice thickness anomalies from common mean, position of the grounding line and the shelf margin for ensemble member 10 and the four different RCM forcing sets in the RCP2.6 (a-d), RCP4.5 (e-h), and RCP8.5 (i-j).

Sea sector.

3.2.5 Ice thickness and grounding line differences in the most sensitive ISM configuration

285 Since both, the magnitude of the ice thickness difference as well as the grounding line position between RCM baseline forcing sets, depends on the chosen ice sheet model parameter choice we illustrate the ice thickness anomalies and grounding line positions for the ensemble member with the largest deviation (ensemble member 10: $\phi_{min} = 6°$, $sia_e = 1.50$, $pQ = 0.8$, $\gamma = 2.5 \times 10^{-5}$) in Fig. 9. For the RCP2.6 and RCP4.5 scenarios, the patterns in ice sheet thickness differences from the common mean are generally similar to the already observed patterns in the present-day equilibrium runs. Simulations forced by MAR

290 mostly show positive thickness anomalies, while COSMO shows mainly negative anomalies. In particular the anomalies at the Transantactic mountains arise from the fact that on a 8km resolution, advection through narrow conduits is poorly resolved which leads to an enhancement of differences in the baseline SMB forcing. Further, RACMO and HIRHAM show a more complex divergent pattern of positive and negative thickness anomalies. However, already in RCP4.5 strong anomalies are observable at the outlet region of Thwaites glacier (c.f. Fig. D4). Here, a retreat in the grounding line compared to present-day

295 observations is observable (c.f. D5). As stated in the above section, the grounding line retreat becomes even more pronounced in the RCP8.5 scenario. Additionally, large differences between the individual forcings in grounding line position but also ice thickness become apparent.

4 Discussion

The aim of this modelling study was to quantify and demonstrate the impact of different baseline SMB and temperature forcings

300 onto the evolution of the Antarctic ice sheet under a 30 000 years present-day equilibrium climate as well as projections using RCP scenarios extended to the year 2300. We now discuss the modelled future sea-level rise contributions and their uncertainties, ice sheet stability and equilibrium states under present-day forcing.

4.1 Uncertainty of Antarctic sea-level contributions due to the choice of RCM baseline forcing

Our simulations suggest differences in projected Antarctic sea-level contributions, due to the choice of present-day SMB and

305 temperature baseline forcing, of $8.7(7.3 - 9.5)$ cm for the RCP8.5 scenario in the year 2100 and 24.3 (16.3 - 46.5) cm in the year 2300. In comparison, the ISMIP6 project demonstrated, that the choice of ISM and GCM forcing creates an uncertainty spread from 9.6 ± 7.2 cm SLE to -3.7 ± 3.4 cm SLE for the end of the 21th century under the RCP8.5 scenario (Seroussi et al., 2020). Although, results of extended ISMIP6 simulations until the year 2300 are not publicly available yet, it is apparent that uncertainties on Antarctic sea-level rise contributions due to the choice of a present-day baseline forcing are on the same order

310 of magnitude as the uncertainties arising from different ISMs and GCM forcings in ISMIP6 (at least for the model and spinup choices considered here). It is important to note that the uncertainty presented here depends partly on the initialization method and the GCM forcing applied. In contrast to this study, in the ISMIP6 protocol models were initialized with different reference present-day forcing fields. Furthermore, various types of model tuning to match present-day observations were applied e.g. nudging or inversion (Seroussi et al., 2020; Nowicki et al., 2020). Specifically, initialization techniques, such as basal friction

315   inversion or nudging, have the capability to incorporate substantial portions of the reference forcing differences into the refined basal friction field. While this could reduce model deviations from the observed state of the ice sheet, it might concurrently give rise to larger differences in a changing climate. Notably, the WAIS is especially sensitive to these minor discrepancies in basal friction due to its overall high sensitivity particularly because of the Marine Ice Sheet Instability (MISI) (DeConto and Pollard, 2016).

320

4.2   Choice of RCM baseline affects the stability of the WAIS in future projections

The complex relationship between the selected RCM forcing data and its impact on future sea-level rise is closely related to the stability of WAIS, particularly the dynamic response of Thwaites and Pine Island Glaciers. This becomes particularly evident in the context of the RCP8.5 scenario. Depending on the choice of RCM baseline forcing large differences in grounding line

325   migration (c.f. Fig. 8) and corresponding ice thickness changes(c.f. Fig. 7, 9) are simulated. This underscores the WAIS's sensitivity to the choice of present-day reference forcing data. This underlines the importance of careful model parameterization and selection of forcing data.

It is important to note that the reference forcing data does not influence whether the WAIS enters an unforced grounding line

330   retreat, but rather modulates the rate of ice loss. The initiation of unforced grounding line retreat seems to be predominantly dependant on the ocean thermal forcing. This is evident from the fast ice loss observed soon after the beginning of the RCP8.5 scenario, in stark contrast to the control runs which exhibit minimal changes (c.f. Fig. D1).

4.3   Millennial-Scale response predisposed by choice of RCM reference forcing

335   To demonstrate the influence of reference SMB and temperature fields on the long-term evolution of WAIS, we presented individual simulation results from our ensemble, as shown in Fig. 5 and Fig. C1. Our simulations clearly indicate that differences in reference SMB and temperature forcing can lead to not only a slow, gradual response of the ice sheet thickness, but also rapid, non-linear responses. This is particularly noteworthy because we limited our parameter set to combinations under which the WAIS remains stable for more than 100 000 years under RACMO forcing, as shown in Fig. 5. However when constant MAR

340   forcing is applied for identical ice sheet model parameters, a collapse of the WAIS is observed (c.f. Fig. 5). In this simulation individual grid boxes unground as shown in Fig. C2, leading to reduced butsstressing and an acceleration in ice outflow. In additional simulations in which we only enforced the stability of the WAIS in RACMO for 15 000 years, we observed many situations where some forcing fields resulted in stable simulations, but some SMB and temperature forcing fields crossed a critical stability threshold, resulting in the long-term collapse of the WAIS in the corresponding simulations, as shown in Fig.

345   C1. In these simulation individual grid boxes unground, leading to reduced butsstressing and an acceleration in ice outflow. Notably, the long term evolution of the ice sheets might also be affected by the thermal spinup. In this study, we only performed

a thermal spinup using the RACMO temperature field. Therefore, restarting from the thermal spinup with an alternative RCM baseline forcing might result in a discontinuity in the forcing which could imprint on the long term evolution of the ice sheet.

4.4 SMB anomalies are imprinted in ice thickness equilibrium

350 The simulated change in sea level-relevant ice mass in the present-day equilibrium simulations demonstrates the expected behavior, where simulations with the highest SMB forcing (e.g. MAR) lead to the largest ice volume (c.f. Fig. 3). The observed spatial distributions of Δh roughly agree with the anomalies observed in the SMB forcing. Regional scale structures in Δh often differ from the underlying SMB anomalies, perhaps unsurprising given the inherent non-linearities of WAIS dynamics. Here we discuss the relationship between regional SMB forcing and quasi-equilibrium state of the ice sheet for individual

355 catchment areas (i.e. IMBIE basins). Averaged over those basins (c.f. Fig. A2, B2), the ice sheet gradually responds to the SMB forcing, with only a few exceptions. One exception is the WAIS in simulations forced with the SMB and temperature fields from RACMO. While we mostly observe small positive SMB anomalies in the forcing for all basins except the Ross basin, the thickness anomalies (Δh) are all negative for those basins. The reason for this might be a shift in the ice divide, which would result in an outflux of ice towards the Ross drainage basin.

360 ### 4.5 Ensemble parameter sensitivity of the RCM impact

In terms of parameter sensitivity in long-term equilibrium simulations, Thwaites and Pine Island Glacier exhibit lower sensitivity than in future projections. This can be attributed to two reasons. Firstly, the present-day forcing applied exposes the Antarctic Ice Sheet (AIS) to weaker climate drivers (e.g. ocean induced melt) than all of the RCP scenarios. Therefore, we would expect the parameter sensitivity to be more similar to the RCP2.6 than the RCP8.5 scenario. Secondly, since we only

365 analyzed simulations where the WAIS was overall stable for more than 100,000 years under RACMO forcing, we excluded most simulations and parameter configurations that could lead to a collapse (c.f. Fig C1), resulting in suppressed variability in this region. The ice sheet wide parameter sensitivity is larger than in future projections, which can be attributed to the long response time of the AIS, especially in vast areas of the East Antarctic Ice Sheet (EAIS), and the much smaller simulation time in the future projections. However, a high parameter sensitivity highlights regions where the interplay between SMB and

370 chosen parameters is highest. Therefore, the model representation of these regions would especially profit if one would narrow down the uncertainty of the surface mass balance forcing.

5 Conclusion

Regional climate model SMB and temperature data are a standard ressource for studies employing large scale ISMs. In this study, we investigated the influence of a set of different RCM products on the evolution and dynamics of the AIS in a 30 000

375 year constant forcing equilibrium simulation as well as in several future projections employing RCP2.6, RCP4.5, and RCP8.5 using a parameter ensemble reflecting various ice sheet sensitivities. Our results demonstrated that although all surface mass balance and temperature products are externally driven by the same reanalysis and simulate the same fields, the impact of their

differences on both ice thickness and grounding line dynamics is considerable. For the long term "quasi-equilibrium" state after 30 ka of simulation, we showed that ice thickness anomalies averaged over the individual IMBIE drainage basins mostly

380   reflect SMB differences between RCMs. However, the differences in SMB forcing can lead to non-linear ice sheet responses on regional scales. For the centennial term projections, our findings indicate that differences mostly arise in and are limited to the vicinity of the grounding line. Our simulations further show that the model-uncertainty for sea level rise projections from the difference in reference present-day forcing is on the same order of magnitude as the uncertainty arising from the choice of ISM and GCM forcing. Additionally, our simulations depict differences in the pacing and timing of grounding line

385   retreat and ice thickness for Thwaites and Pine Island Glacier under intermediate and high emission scenarios (i.e. RCP4.5, RCP8.5). Our sensitivity analysis, indicates that the imprint of the SMB forcing on the ice thickness is especially dependent on the chosen parameters for the ISM (model sensitivity). Our long term equilibrium study additionally indicates that the difference in the SMB products is large enough to result in long term instabilities of the WAIS in one forcing set, while long term WAIS stability can be observed in another. Our study displays the large impact of the choice of a reference present-day

390   forcing onto projections of ice sheet evolution, however this sensitivity is model dependent and should be explored on a case-by-case basis. Prospectively, a more rigorous approach employing a wider sweep of parameters, more sophisticated ice sheet initialisation methods (less model drift) and a larger set of GCM and RCM climate projections, would be desirable. Yet, here we demonstrate the problem that occurs due to the spread in RCM products, the order of magnitude of this uncertainty and potential implications on the stability of the ice sheet.

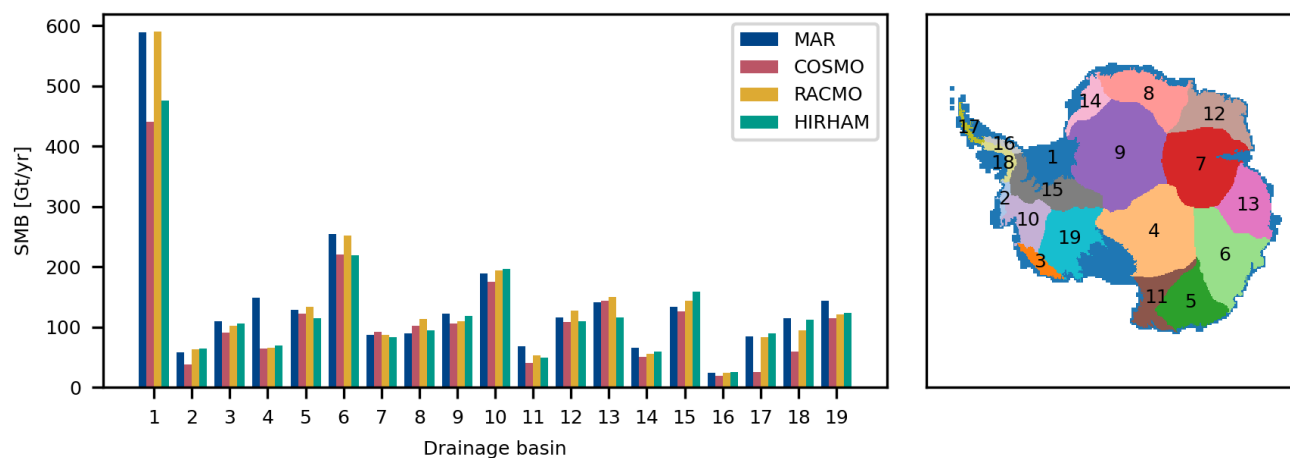## Appendix A: Annual SMB in the different drainage areas

395

Figure A1. Annual SMB for the 19 IMBIE drainage areas.Corresponding areas are marked on the map. Please be aware that area 1 includes all shelf ice areas.
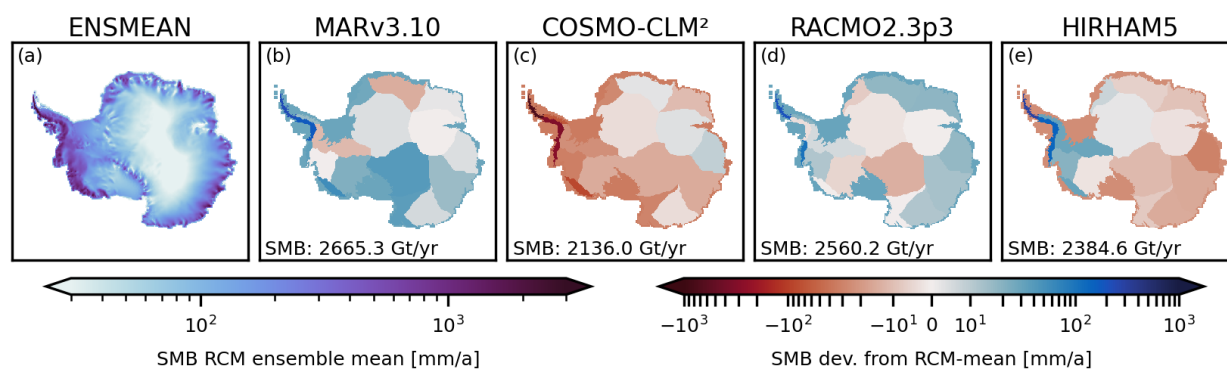

Figure A2. Surface mass balance (SMB) of the (a) multi-RCM mean and anomalies of the (b) MARv3.10, (c) COSMO-CLM2, (d) RACMO2.3p3, and (e) HIRHAM5 regional climate model from this mean averaged over the individual IMBIE basins.

Appendix B: Ice thickness difference to PD observations for PD-equilibrium
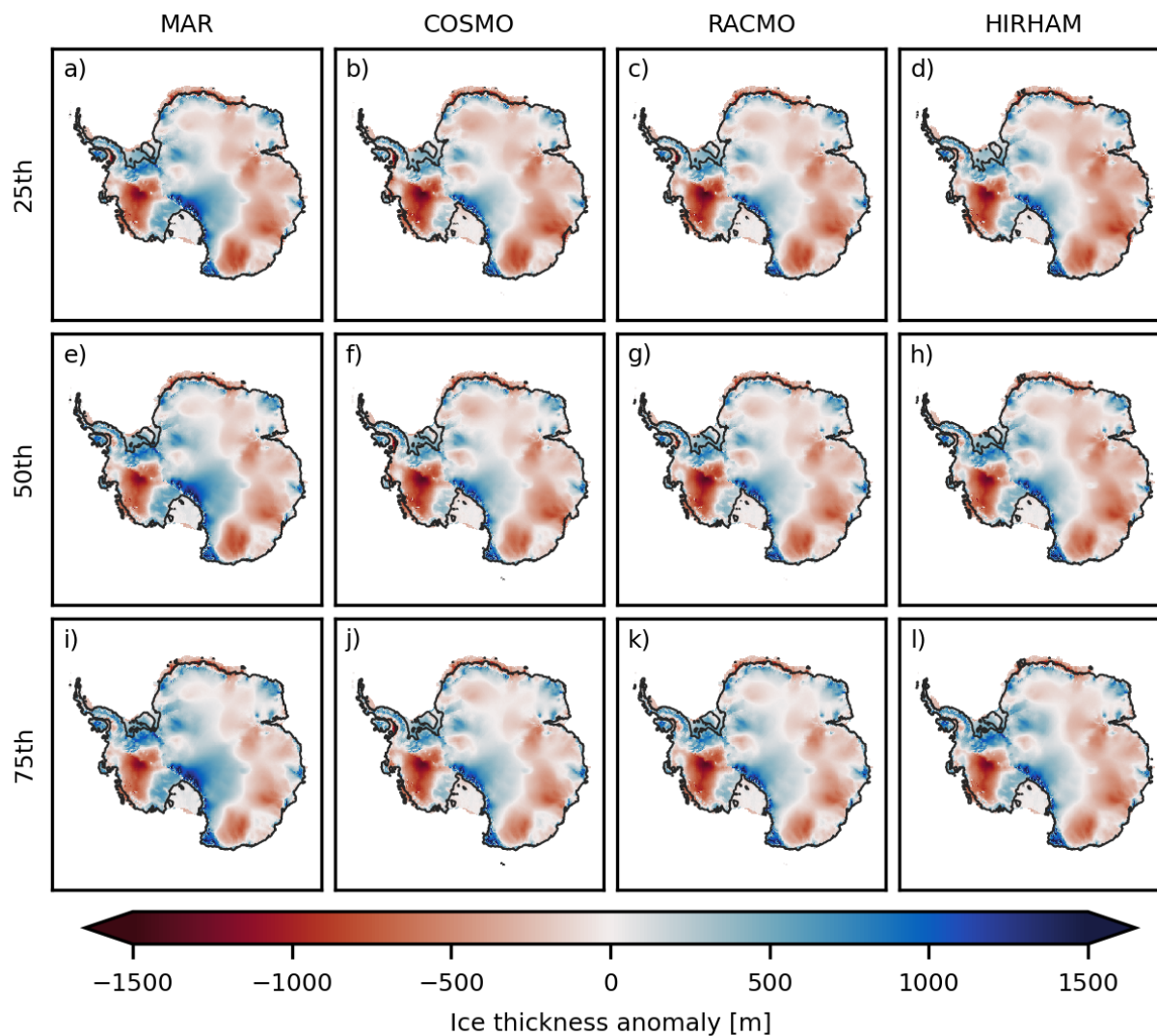
Figure B1. Ice thickness anomalies towards present-day observations after 30 000 years under the given RCM SMB. a)-d) shows the 25th, e)-h) the 50th, and i)-l) the 75th percentile of the ensemble.
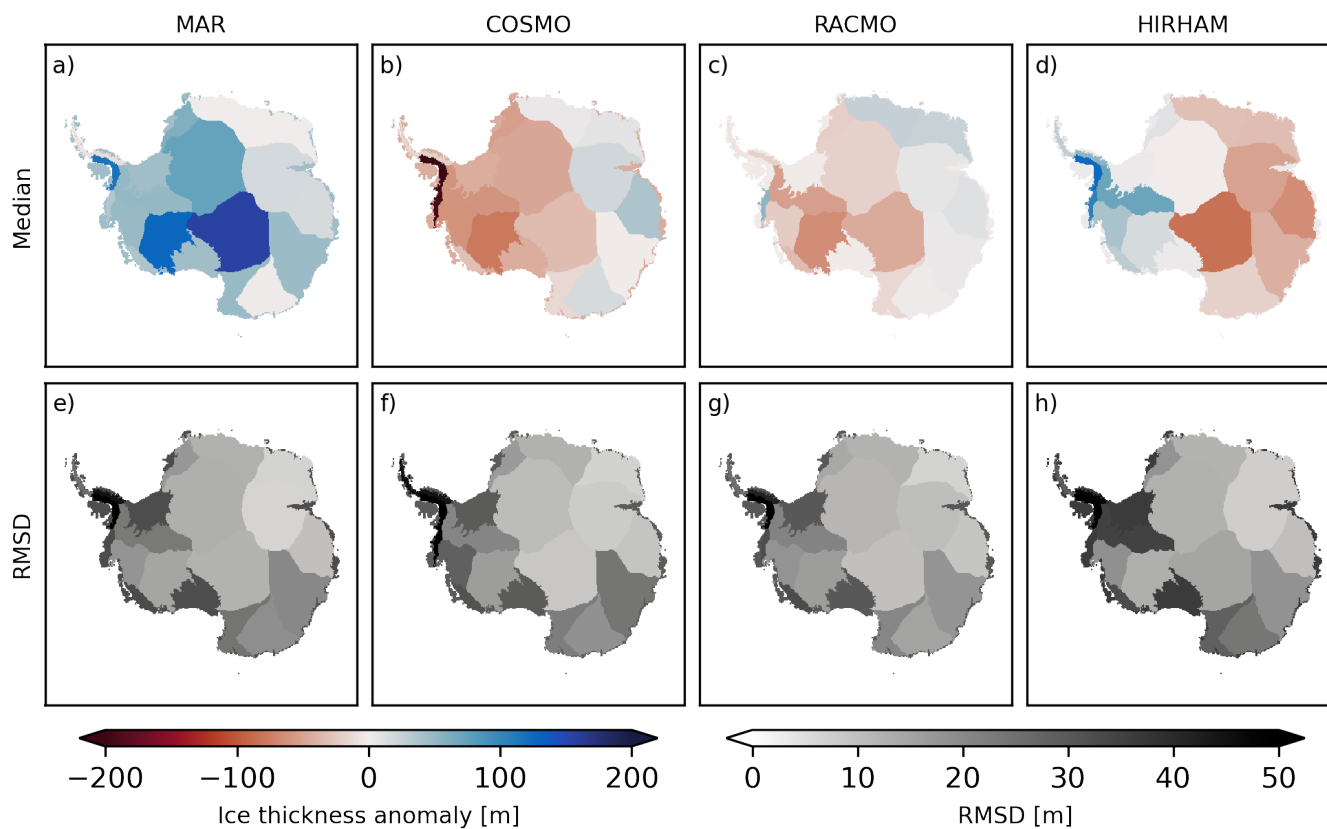
Figure B2. Ice thickness anomalies from common mean (a-d), position of the simulated (purple) and observed (grey) grounding line for the present-day equilibrium simulations. Root mean square error (RMSD) of the individual ensemble members from the median (e-h). All values averaged over the individual IMBIE drainage basins.
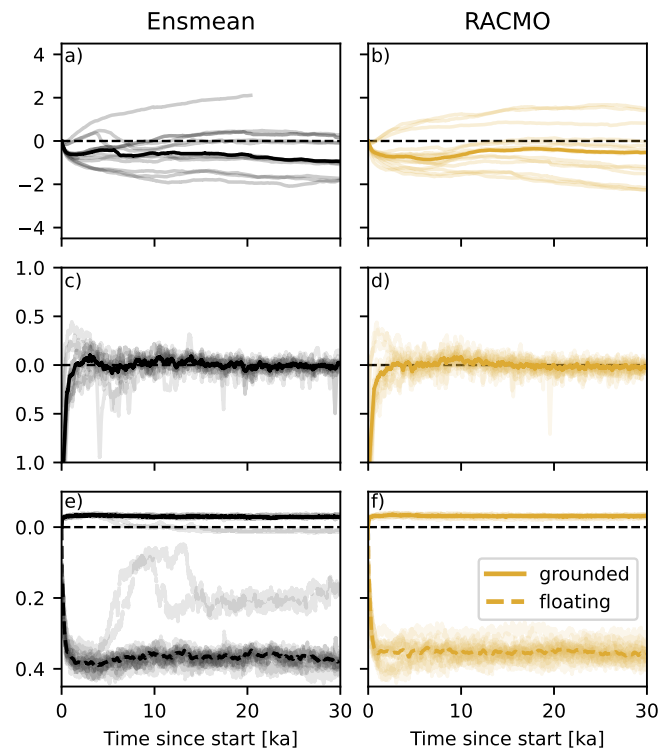
Figure B3. Time series of the total ice mass change (a,b), the annual rate of change (c,d), and the fraction of grounded (solid line) and floating (dashed line) ice area (e,f) relative to present-day observations for the simulations forced by the mean of all four RCM products (referred to as ensmean) and simulations forced by RACMO. Bold line shows ensemble median while shaded lines indicate the individual ensemble members. In two of the simulations forced by ensmean, a collapse of the WAIS is observable. Additionally, one simulation exceeded the upper boundary of the computational domain after ca. 20 thousand years

Ice thickness   Ice thickness anomaly
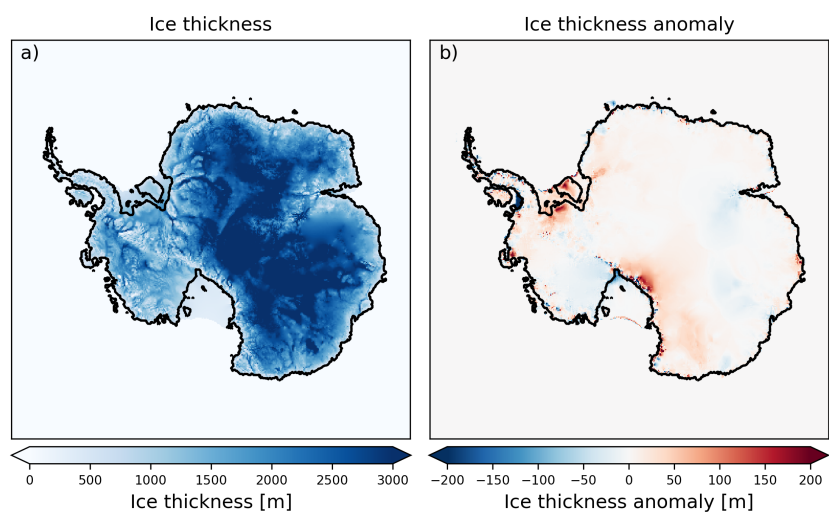
Figure B4. Median ice thickness of the forcing ensemble mean simulations (a) and the median ice thickness anomalies when compared with the mean of the individual forcing simulations (b).

Appendix C: Selected individual runs

	sia_e	pQ	γ	$\phi_{till,min}$
AX	1.25	0.80	3.0×10^{-5}	2°
AY	1.25	0.75	2.0×10^{-5}	4°
CX	1.0	0.80	3.5×10^{-5}	2°
CY	1.0	0.80	4.0×10^{-5}	2°
CZ	1.25	0.80	4.0×10^{-5}	2°

Table C1. Parameter configurations used in Fig. 5 (AX,AY) and Fig. C1 (CX, CY, CZ).
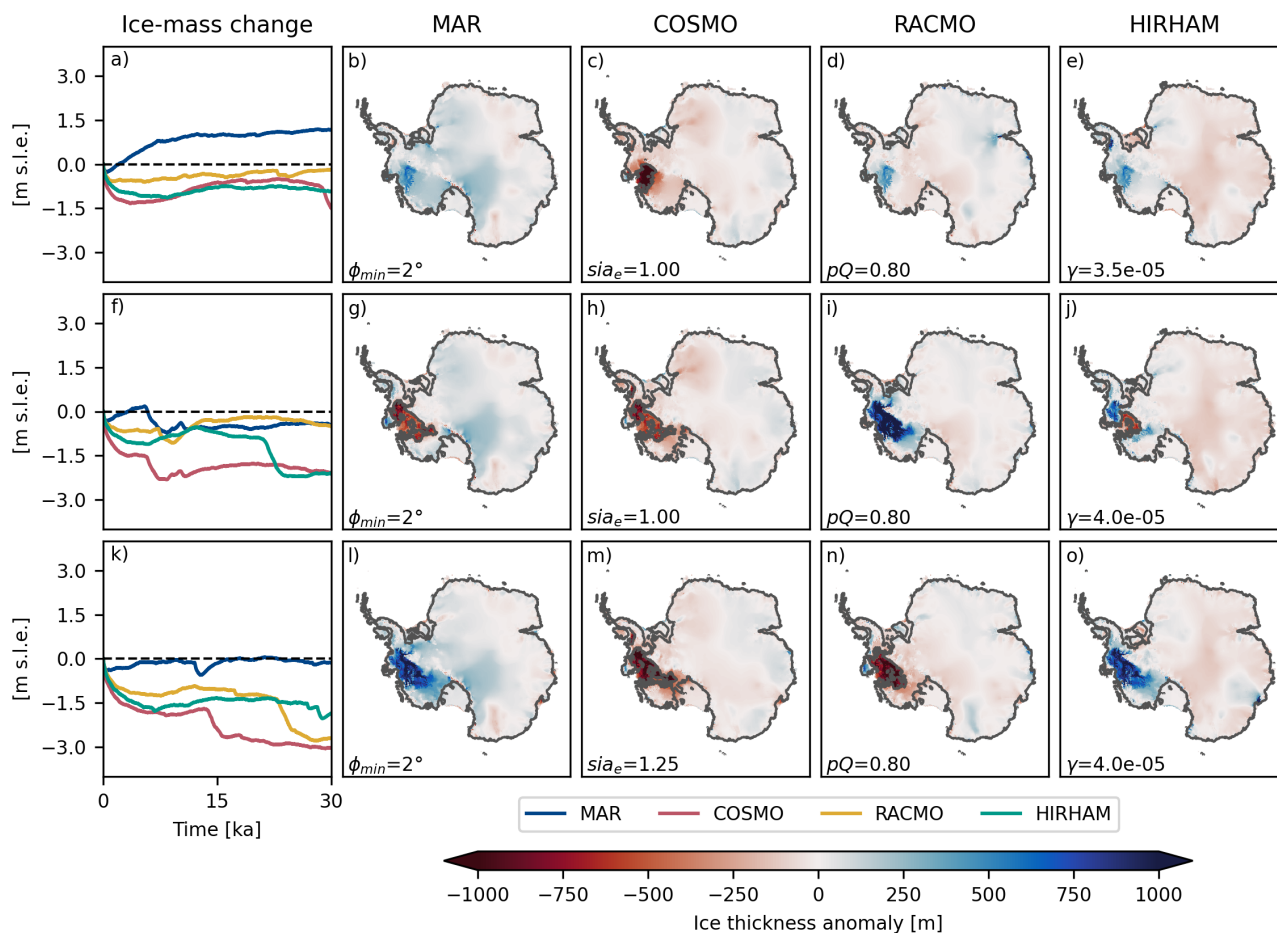
Figure C1. Evolution of the sea level change relevant ice masses (a,f,k) over the simulation period and ice thickness differences from the common mean as well as grounding line position (purple line) at the end of the simulation (b-e, g-j,l-o). The parameters of the here presented simulations are not specially selected to ensure ice sheet stability for 100 kyrs under RACMO forcing but only ensure stability under RACMO forcing for 15 kyrs. Panel a-e show the results of the simulation with $\phi_{min} = 2°$, $sia_e = 1.0$, $pQ = 0.8$, $\gamma = 3.5 \times 10^{-5}$. Panel f-j show the results the simulation with $\phi_{min} = 2°$, $sia_e = 1.0$, $pQ = 0.8$, $\gamma = 4.0 \times 10^{-5}$. Panel k-o show the results the simulation with $\phi_{min} = 2°$, $sia_e = 1.25$, $pQ = 0.8$, $\gamma = 4.0 \times 10^{-5}$.
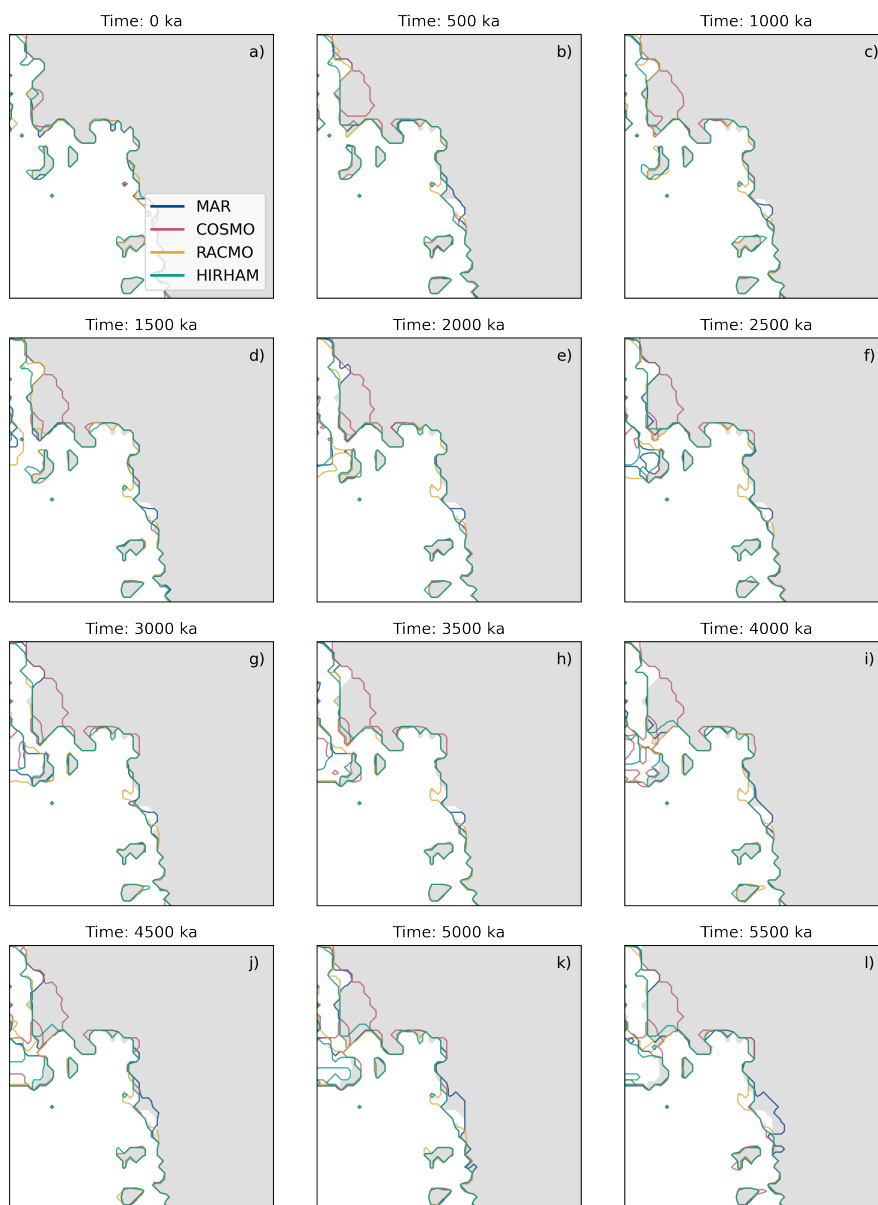
Figure C2. Evolution of the grounding line at thwaites glacier for ensemble member AY in time steps of 500 years. The grey shaded patches represent the present-day grounding line position. The plot indicates that an early grounding line retreat of the simulation forced by the MAR model leads to a faster and faster retreat of the grounding line, causing the later collapse of WAIS in this simulation as seen in Fig. 5.

Appendix D: Future projections

Starting from 1860 all simulations show a minor ice loss together with an increase in grounded and a corresponding decrease
in floating ice area fraction due to an advance of the grounding line. The loss in ice mass is highest for models forced with
the COSMO climatology and lowest for simulations forced by MAR. From 2005 onwards, a decrease in ice mass relative to
the control run (dashed lines) is simulated in all scenarios. COSMO and MAR being the end members, showing the largest
and smallest loss of ice. This is consistent with the integrated average Antarctic SMB produced by COSMO and MAR. For
this period 2005-2300 a reduction on both grounded and floating ice area fraction is suggested by the model. However, in the
RCP2.6 scenario the loss in floating ice area fraction is almost identical to the control run. Overall, compared to the control run
the observed changes in the RCP2.6 and RCP4.5 scenarios are relatively small. In contrast, the changes in the RCP8.5 scenario
are significantly larger due to strong ocean and atmospheric warming and associated mass losses due to ice shelf and surface
melt. From 2005 to approximately 2200 the rate of mass loss is accelerating, which is reflected in the total ice mass change as
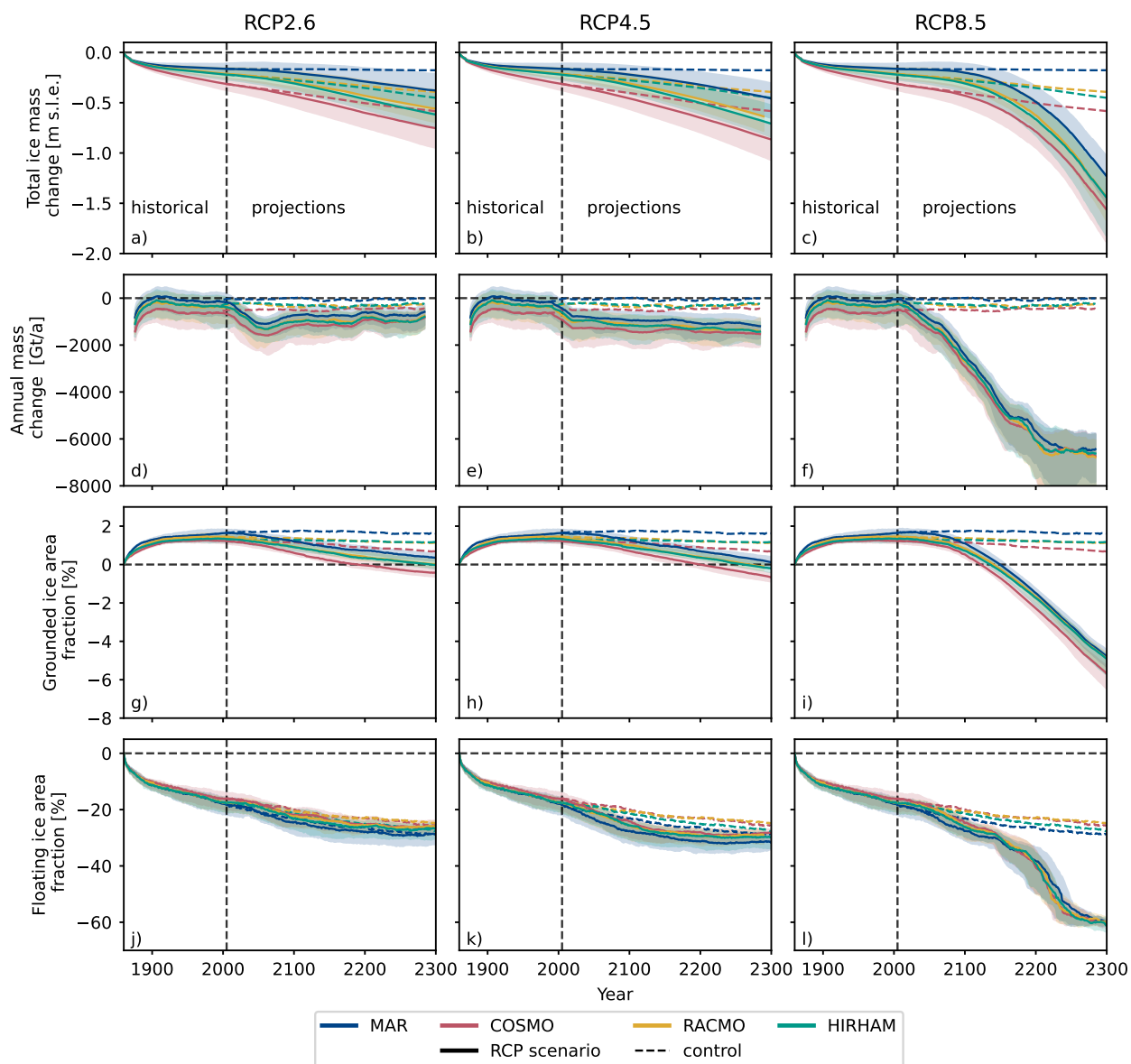well as the grounded and floating ice area.

Figure D1. Time series of the total ice mass change (a-c), the annual rate of change (d-f), and the fraction of grounded (g-i) and floating (j-l) ice area fraction relative to observations for the four different RCM forcing fields and the RCP2.6, RCP4.5, and RCP8.5 climate scenarios. Dashed lines represent the control runs with constant 2005 forcing. Shadings indicate the 25th to 75th quantile.
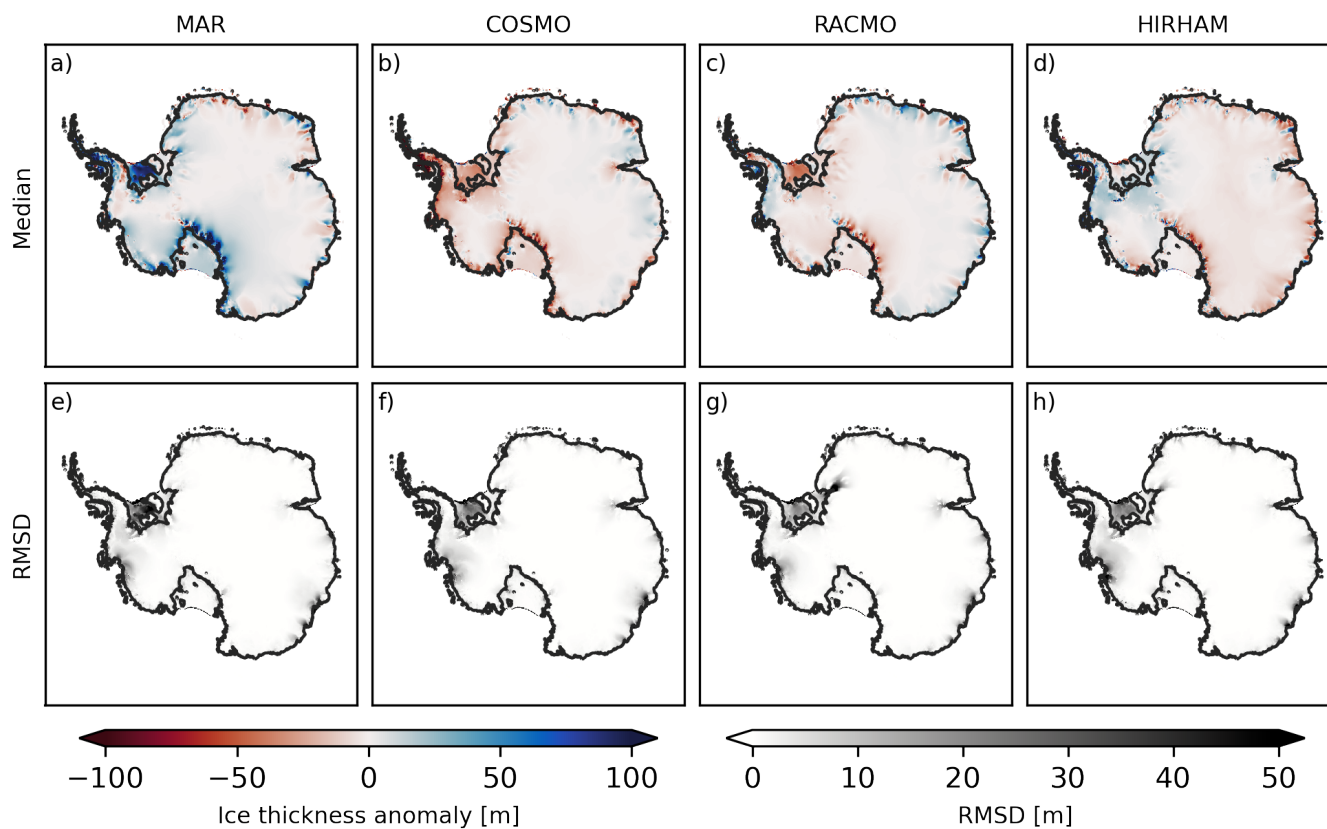
Figure D2. Ice thickness anomalies from common mean (a-d), position of the simulated (purple) and observed (grey) grounding line for the RCP2.6 future projection. Root mean square error (RMSD) of the individual ensemble members from the median (e-h).
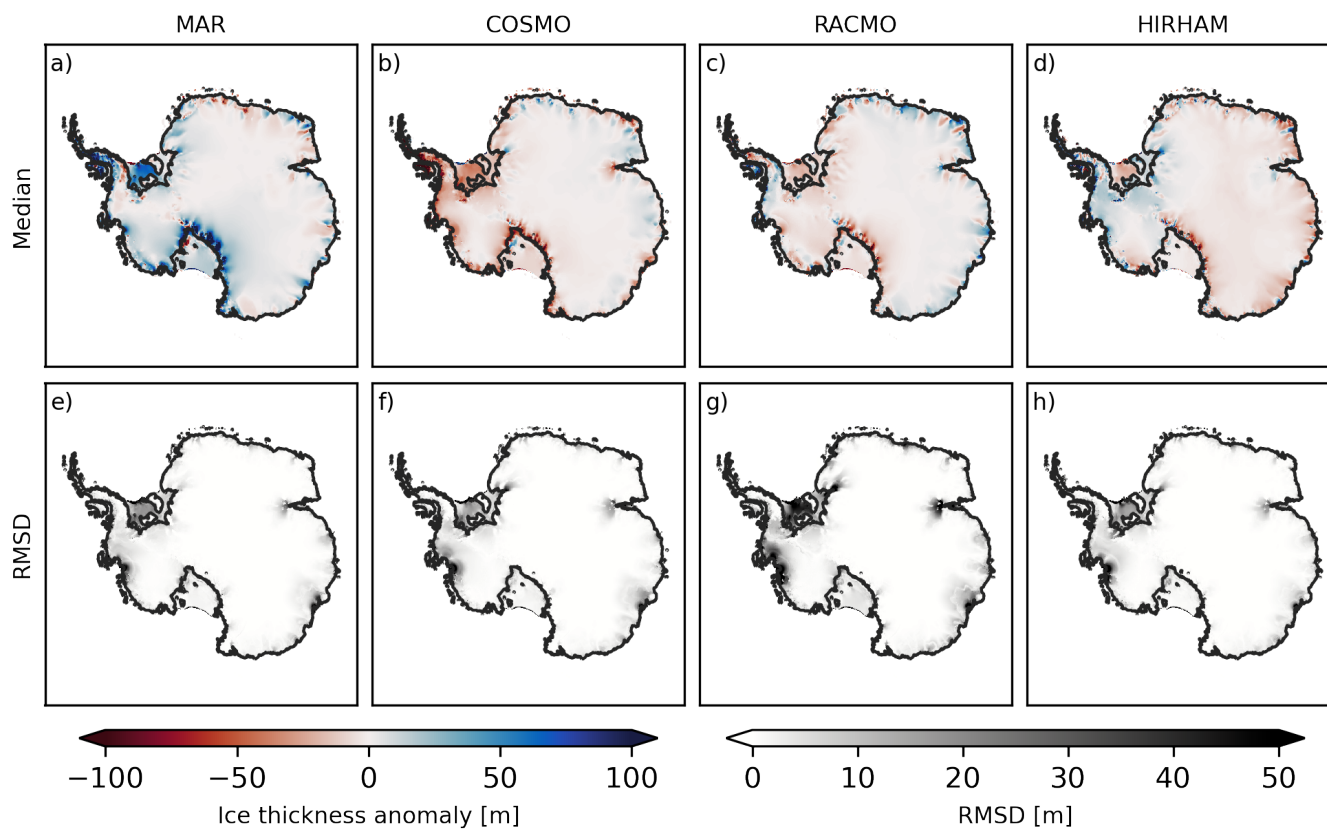
Figure D3. Ice thickness anomalies from common mean (a-d), position of the simulated (purple) and observed (grey) grounding line for the RCP4.5 future projection. Root mean square error (RMSD) of the individual ensemble members from the median (e-h).
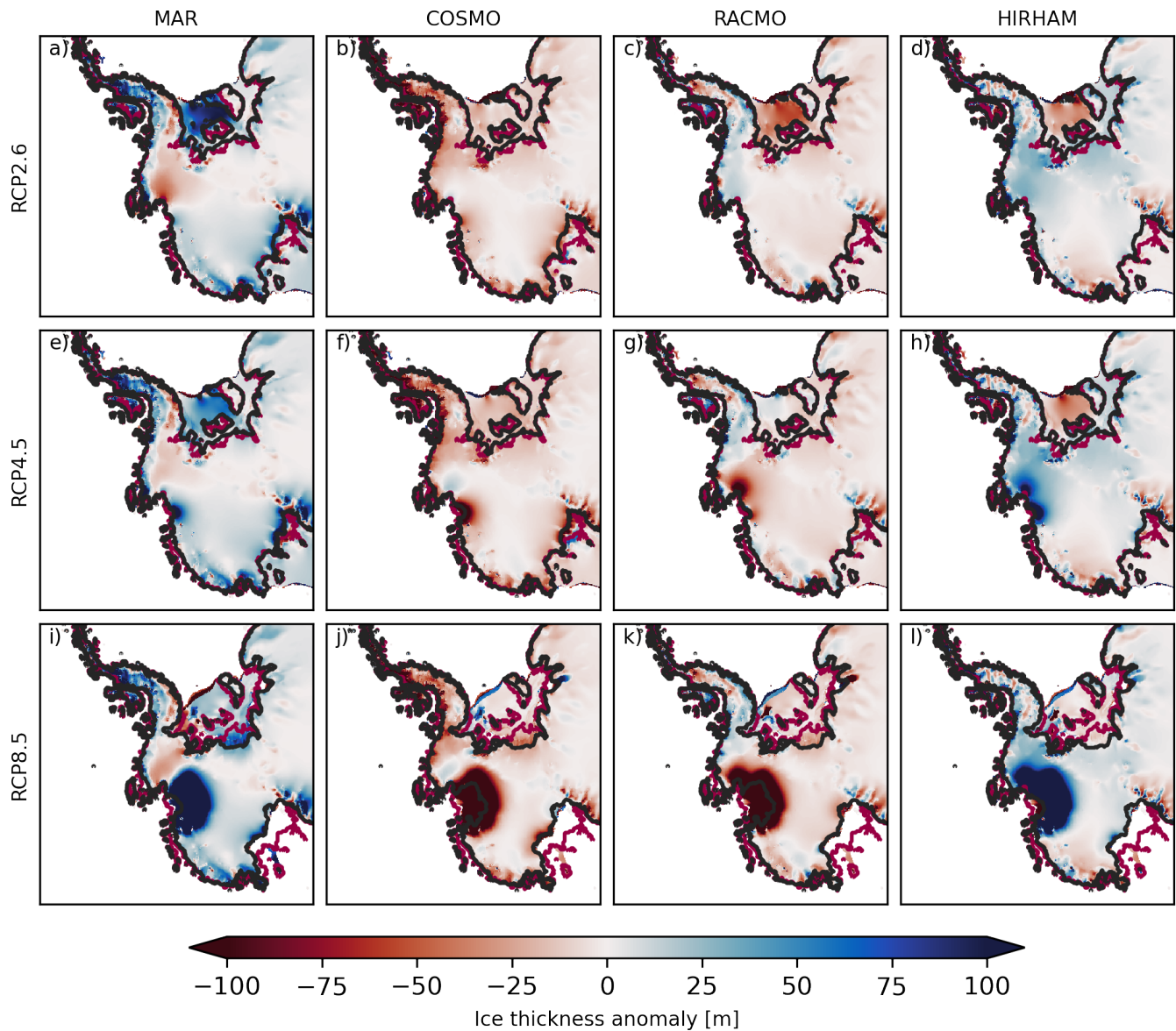
Figure D4. WAIS thickness anomalies from common mean, position of the grounding line and the shelf margin for the four different RCM forcing sets in the RCP2.6 (a-d), RCP4.5 (e-h), and RCP8.5 (i-j).
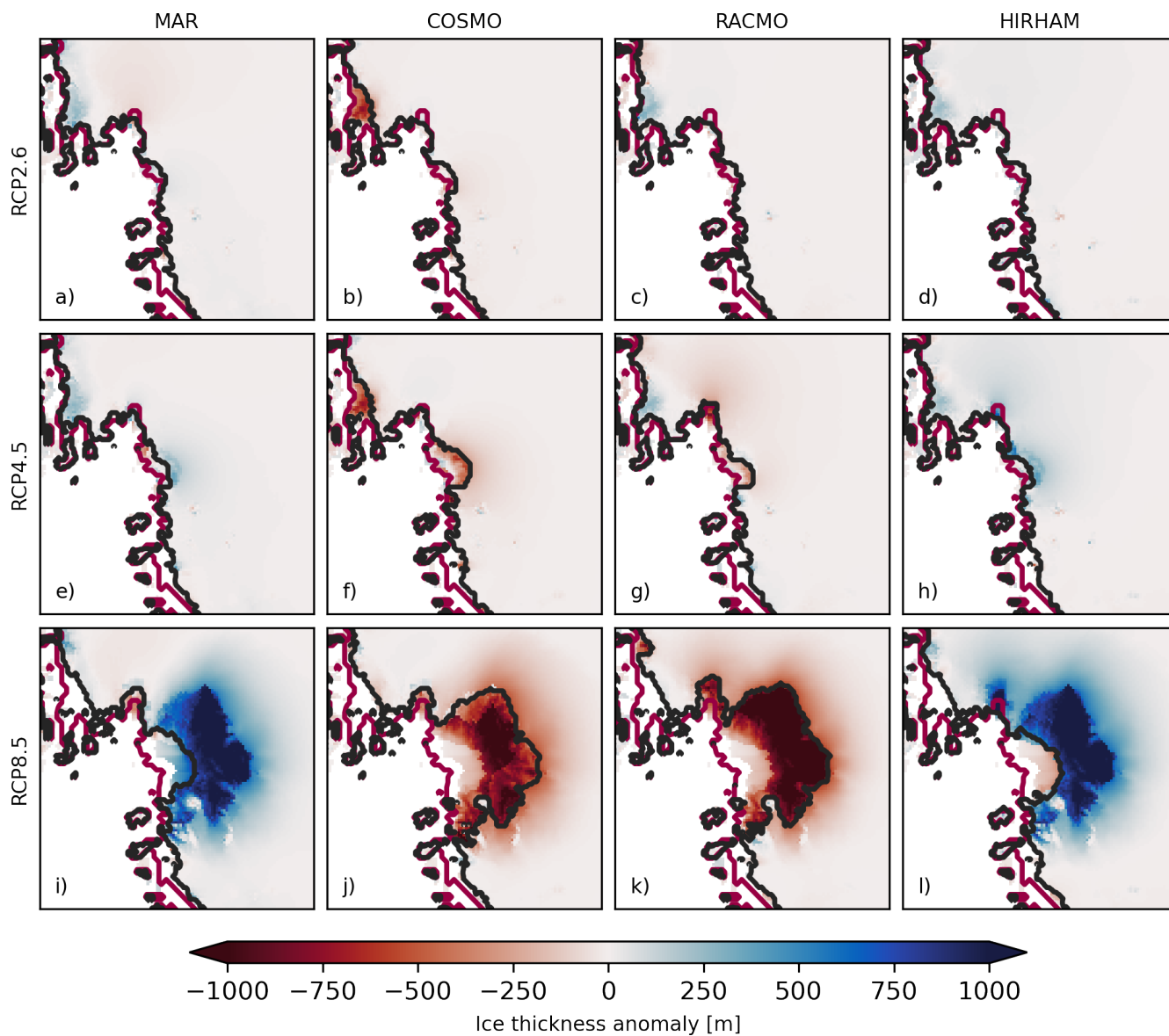
Figure D5. Ice thickness anomalies from common mean at thwaites glacier outlet, position of the grounding line and the shelf margin for the four different RCM forcing sets in the RCP2.6 (a-d), RCP4.5 (e-h), and RCP8.5 (i-j).

Author contributions. CW, JS, and TS conceptualized this study, decided on the methodology, analysed the data, edited and wrote this

415   manuscript. CW lead the writing of the manuscript, ran the simulations and visualized the data under supervision of JS and TS

Competing interests. The authors declare that there are no competing interests.

References

Albrecht, T., Winkelmann, R., and Levermann, A.: Glacial-cycle simulations of the Antarctic Ice Sheet with the Parallel Ice Sheet Model
425   (PISM) – Part 1: Boundary conditions and climatic forcing, The Cryosphere, 14, 599–632, https://doi.org/10.5194/tc-14-599-2020, 2020.

Aschwanden, A., Aðalgeirsdóttir, G., and Khroulev, C.: Hindcasting to measure ice sheet model sensitivity to initial states, The Cryosphere,
7, 1083–1093, https://doi.org/10.5194/tc-7-1083-2013, publisher: Copernicus GmbH, 2013.

Bamber, J. L., Riva, R. E. M., Vermeersen, B. L. A., and LeBrocq, A. M.: Reassessment of the Potential Sea-Level Rise from a Collapse of
the West Antarctic Ice Sheet, Science, 324, 901–903, https://doi.org/10.1126/science.1169335, 2009.

430   Bevan, S., Cornford, S., Gilbert, L., Otosaka, I., Martin, D., and Surawy-Stepney, T.: Amundsen Sea Embayment ice-sheet mass-
loss predictions to 2050 calibrated using observations of velocity and elevation change, Journal of Glaciology, pp. 1–11,
https://doi.org/10.1017/jog.2023.57, 2023.

Boyer, T. P., Baranova, O. K., Coleman, C., Garcia, H. E., Grodsky, A., Locarnini, R. A., Mishonov, A. V., Paver, C. R., Reagan, J. R., Seidov,
D., Smolyar, I. V., Weathers, K. W., and Zweng, M. M.: WORLD OCEAN DATABASE 2018, 2018.

435   Bueler, E. and Brown, J.: Shallow shelf approximation as a "sliding law" in a thermomechanically coupled ice sheet model, Journal of
Geophysical Research, 114, F03 008, https://doi.org/10.1029/2008JF001179, 2009.

Bulthuis, K., Arnst, M., Sun, S., and Pattyn, F.: Uncertainty quantification of the multi-centennial response of the Antarctic ice sheet to
climate change, The Cryosphere, 13, 1349–1380, https://doi.org/10.5194/tc-13-1349-2019, publisher: Copernicus GmbH, 2019.

Cuffey, K. and Paterson, W. S. B.: The physics of glaciers, Butterworth-Heinemann/Elsevier, Burlington, MA, 4th ed edn., oCLC:
440   ocn488732494, 2010.

DeConto, R. M. and Pollard, D.: Contribution of Antarctica to past and future sea-level rise, Nature, 531, 591–597,
https://doi.org/10.1038/nature17145, 2016.

Dee, D. P., Uppala, S. M., Simmons, A. J., Berrisford, P., Poli, P., Kobayashi, S., Andrae, U., Balmaseda, M. A., Balsamo, G., Bauer,
P., Bechtold, P., Beljaars, A. C. M., van de Berg, L., Bidlot, J., Bormann, N., Delsol, C., Dragani, R., Fuentes, M., Geer, A. J., Haim-
445   berger, L., Healy, S. B., Hersbach, H., Hólm, E. V., Isaksen, L., Kållberg, P., Köhler, M., Matricardi, M., McNally, A. P., Monge-Sanz,
B. M., Morcrette, J.-J., Park, B.-K., Peubey, C., de Rosnay, P., Tavolato, C., Thépaut, J.-N., and Vitart, F.: The ERA-Interim reanalysis:
configuration and performance of the data assimilation system, Quarterly Journal of the Royal Meteorological Society, 137, 553–597,
https://doi.org/10.1002/qj.828, _eprint: https://onlinelibrary.wiley.com/doi/pdf/10.1002/qj.828, 2011.

Ettema, J., van den Broeke, M. R., van Meijgaard, E., and van de Berg, W. J.: Climate of the Greenland ice sheet using a high-resolution
450   climate model – Part 2: Near-surface climate and energy balance, The Cryosphere, 4, 529–544, https://doi.org/10.5194/tc-4-529-2010,
2010.

Hansen, N., Langen, P. L., Boberg, F., Forsberg, R., Simonsen, S. B., Thejll, P., Vandecrux, B., and Mottram, R.: Downscaled surface
mass balance in Antarctica: impacts of subsurface processes and large-scale atmospheric circulation, The Cryosphere, 15, 4315–4333,
https://doi.org/10.5194/tc-15-4315-2021, 2021.

455   Hansen, N., Simonsen, S. B., Boberg, F., Kittel, C., Orr, A., Souverijns, N., van Wessem, J. M., and Mottram, R.: Brief communi-
cation: Impact of common ice mask in surface mass balance estimates over the Antarctic ice sheet, The Cryosphere, 16, 711–718,
https://doi.org/10.5194/tc-16-711-2022, publisher: Copernicus GmbH, 2022.

Hooijer, A. and Vernimmen, R.: Global LiDAR land elevation data reveal greatest sea-level rise vulnerability in the tropics, Nature Commu-
nications, 12, 3592, https://doi.org/10.1038/s41467-021-23810-9, number: 1 Publisher: Nature Publishing Group, 2021.

460   IPCC: The Ocean and Cryosphere in a Changing Climate: Special Report of the Intergovernmental Panel on Climate Change, Cambridge
        University Press, 1 edn., https://doi.org/10.1017/9781009157964, 2022.

      Jones, A. C., Hawcroft, M. K., Haywood, J. M., Jones, A., Guo, X., and Moore, J. C.: Regional Climate Impacts of Stabilizing
        Global Warming at 1.5 K Using Solar Geoengineering, Earth's Future, 6, 230–251, https://doi.org/10.1002/2017EF000720, _eprint:
        https://onlinelibrary.wiley.com/doi/pdf/10.1002/2017EF000720, 2018.

465   Kittel, C., Amory Charles, Agosta Cécile, and Fettweis Xavier: MARv3.10 outputs: What is the Surface Mass Balance of Antarctica? An
        Intercomparison of Regional Climate Model Estimates, https://doi.org/10.5281/zenodo.5195636, 2020.

      Lenaerts, J. T. M., van den Broeke, M. R., Déry, S. J., van Meijgaard, E., van de Berg, W. J., Palm, S. P., and Sanz Rodrigo, J.: Modeling drift-
        ing snow in Antarctica with a regional climate model: 1. Methods and model evaluation, Journal of Geophysical Research: Atmospheres,
        117, https://doi.org/10.1029/2011JD016145, _eprint: https://onlinelibrary.wiley.com/doi/pdf/10.1029/2011JD016145, 2012.

470   Li, D., DeConto, R. M., and Pollard, D.: Climate model differences contribute deep uncertainty in future Antarctic ice loss, Science Advances,
        9, eadd7082, https://doi.org/10.1126/sciadv.add7082, publisher: American Association for the Advancement of Science, 2023.

      Martin, M. A., Winkelmann, R., Haseloff, M., Albrecht, T., Bueler, E., Khroulev, C., and Levermann, A.: The Potsdam Parallel
        Ice Sheet Model (PISM-PIK) – Part 2: Dynamic equilibrium simulation of the Antarctic ice sheet, The Cryosphere, 5, 727–740,
        https://doi.org/10.5194/tc-5-727-2011, 2011.

475   Morlighem, M., Williams, C. N., Rignot, E., An, L., Arndt, J. E., Bamber, J. L., Catania, G., Chauché, N., Dowdeswell, J. A., Dorschel,
        B., Fenty, I., Hogan, K., Howat, I., Hubbard, A., Jakobsson, M., Jordan, T. M., Kjeldsen, K. K., Millan, R., Mayer, L., Mouginot, J.,
        Noël, B. P. Y., O'Cofaigh, C., Palmer, S., Rysgaard, S., Seroussi, H., Siegert, M. J., Slabon, P., Straneo, F., van den Broeke, M. R.,
        Weinrebe, W., Wood, M., and Zinglersen, K. B.: BedMachine v3: Complete Bed Topography and Ocean Bathymetry Mapping of
        Greenland From Multibeam Echo Sounding Combined With Mass Conservation, Geophysical Research Letters, 44, 11,051–11,061,
480   https://doi.org/10.1002/2017GL074954, _eprint: https://onlinelibrary.wiley.com/doi/pdf/10.1002/2017GL074954, 2017.

      Morlighem, M., Rignot, E., Binder, T., Blankenship, D., Drews, R., Eagles, G., Eisen, O., Ferraccioli, F., Forsberg, R., Fretwell, P., Goel,
        V., Greenbaum, J. S., Gudmundsson, H., Guo, J., Helm, V., Hofstede, C., Howat, I., Humbert, A., Jokat, W., Karlsson, N. B., Lee, W. S.,
        Matsuoka, K., Millan, R., Mouginot, J., Paden, J., Pattyn, F., Roberts, J., Rosier, S., Ruppel, A., Seroussi, H., Smith, E. C., Steinhage, D.,
        Sun, B., Broeke, M. R. v. d., Ommen, T. D. v., Wessem, M. v., and Young, D. A.: Deep glacial troughs and stabilizing ridges unveiled
485   beneath the margins of the Antarctic ice sheet, Nature Geoscience, 13, 132–137, https://doi.org/10.1038/s41561-019-0510-8, number: 2
        Publisher: Nature Publishing Group, 2020.

      Mottram, R., Hansen, N., Kittel, C., van Wessem, J. M., Agosta, C., Amory, C., Boberg, F., van de Berg, W. J., Fettweis, X., Gossart, A., van
        Lipzig, N. P. M., van Meijgaard, E., Orr, A., Phillips, T., Webster, S., Simonsen, S. B., and Souverijns, N.: What is the surface mass balance
        of Antarctica? An intercomparison of regional climate model estimates, The Cryosphere, 15, 3751–3784, https://doi.org/10.5194/tc-15-
490   3751-2021, 2021.

      Nowicki, S., Goelzer, H., Seroussi, H., Payne, A. J., Lipscomb, W. H., Abe-Ouchi, A., Agosta, C., Alexander, P., Asay-Davis, X. S., Barthel,
        A., Bracegirdle, T. J., Cullather, R., Felikson, D., Fettweis, X., Gregory, J. M., Hattermann, T., Jourdain, N. C., Kuipers Munneke, P.,
        Larour, E., Little, C. M., Morlighem, M., Nias, I., Shepherd, A., Simon, E., Slater, D., Smith, R. S., Straneo, F., Trusel, L. D., van den
        Broeke, M. R., and van de Wal, R.: Experimental protocol for sea level projections from ISMIP6 stand-alone ice sheet models, The
495   Cryosphere, 14, 2331–2368, https://doi.org/10.5194/tc-14-2331-2020, publisher: Copernicus GmbH, 2020.

      Oleson, K., Lawrence, M., Bonan, B., Drewniak, B., Huang, M., Koven, D., Levis, S., Li, F., Riley, J., Subin, M., Swenson, S., Thorn-
        ton, E., Bozbiyik, A., Fisher, R., Heald, L., Kluzek, E., Lamarque, J.-F., Lawrence, J., Leung, R., Lipscomb, W., Muszala, P., Ric-

ciuto, M., Sacks, J., Sun, Y., Tang, J., and Yang, Z.-L.: Technical description of version 4.5 of the Community Land Model (CLM), https://doi.org/10.5065/D6RR1W7M, 2013.

500 Otosaka, I. N., Shepherd, A., Ivins, E. R., Schlegel, N.-J., Amory, C., van den Broeke, M. R., Horwath, M., Joughin, I., King, M. D., Krinner, G., Nowicki, S., Payne, A. J., Rignot, E., Scambos, T., Simon, K. M., Smith, B. E., Sørensen, L. S., Velicogna, I., Whitehouse, P. L., A, G., Agosta, C., Ahlstrøm, A. P., Blazquez, A., Colgan, W., Engdahl, M. E., Fettweis, X., Forsberg, R., Gallée, H., Gardner, A., Gilbert, L., Gourmelen, N., Groh, A., Gunter, B. C., Harig, C., Helm, V., Khan, S. A., Kittel, C., Konrad, H., Langen, P. L., Lecavalier, B. S., Liang, C.-C., Loomis, B. D., McMillan, M., Melini, D., Mernild, S. H., Mottram, R., Mouginot, J., Nilsson, J., Noël, B., Pattle, M. E., Peltier,
505 W. R., Pie, N., Roca, M., Sasgen, I., Save, H. V., Seo, K.-W., Scheuchl, B., Schrama, E. J. O., Schröder, L., Simonsen, S. B., Slater, T., Spada, G., Sutterley, T. C., Vishwakarma, B. D., van Wessem, J. M., Wiese, D., van der Wal, W., and Wouters, B.: Mass balance of the Greenland and Antarctic ice sheets from 1992 to 2020, Earth System Science Data, 15, 1597–1616, https://doi.org/10.5194/essd-15-1597-2023, publisher: Copernicus GmbH, 2023.

Pattyn, F.: The paradigm shift in Antarctic ice sheet modelling, Nature Communications, 9, 2728, https://doi.org/10.1038/s41467-018-05003-
510 z, number: 1 Publisher: Nature Publishing Group, 2018.

Pollard, D. and DeConto, R. M.: A simple inverse method for the distribution of basal sliding coefficients under ice sheets, applied to Antarctica, The Cryosphere, 6, 953–971, https://doi.org/10.5194/tc-6-953-2012, 2012.

Reese, R., Albrecht, T., Mengel, M., Asay-Davis, X., and Winkelmann, R.: Antarctic sub-shelf melt rates via PICO, The Cryosphere, 12, 1969–1985, https://doi.org/10.5194/tc-12-1969-2018, publisher: Copernicus GmbH, 2018.

515 Reese, R., Garbe, J., Hill, E. A., Urruty, B., Naughten, K. A., Gagliardini, O., Durand, G., Gillet-Chaulet, F., Chandler, D., Langebroek, P. M., and Winkelmann, R.: The stability of present-day Antarctic grounding lines – Part B: Possible commitment of regional collapse under current climate, preprint, Ice sheets/Numerical Modelling, https://doi.org/10.5194/tc-2022-105, 2022.

Ridder, K. D. and Gallée, H.: Land Surface–Induced Regional Climate Change in Southern Israel, Journal of Applied Meteorology and Climatology, 37, 1470–1485, https://doi.org/10.1175/1520-0450(1998)037<1470:LSIRCC>2.0.CO;2, publisher: American Meteorological
520 Society Section: Journal of Applied Meteorology and Climatology, 1998.

Rignot, E., Mouginot, J., Scheuchl, B., van den Broeke, M., van Wessem, M. J., and Morlighem, M.: Four decades of Antarctic Ice Sheet mass balance from 1979–2017, Proceedings of the National Academy of Sciences, 116, 1095–1103, https://doi.org/10.1073/pnas.1812883116, publisher: Proceedings of the National Academy of Sciences, 2019.

Schoof, C.: Ice sheet grounding line dynamics: Steady states, stability, and hysteresis, Journal of Geophysical Research: Earth Surface, 112,
525 https://doi.org/10.1029/2006JF000664, _eprint: https://onlinelibrary.wiley.com/doi/pdf/10.1029/2006JF000664, 2007.

Seroussi, H., Nowicki, S., Payne, A. J., Goelzer, H., Lipscomb, W. H., Abe-Ouchi, A., Agosta, C., Albrecht, T., Asay-Davis, X., Barthel, A., Calov, R., Cullather, R., Dumas, C., Galton-Fenzi, B. K., Gladstone, R., Golledge, N. R., Gregory, J. M., Greve, R., Hattermann, T., Hoffman, M. J., Humbert, A., Huybrechts, P., Jourdain, N. C., Kleiner, T., Larour, E., Leguy, G. R., Lowry, D. P., Little, C. M., Morlighem, M., Pattyn, F., Pelle, T., Price, S. F., Quiquet, A., Reese, R., Schlegel, N.-J., Shepherd, A., Simon, E., Smith, R. S., Straneo, F., Sun, S.,
530 Trusel, L. D., Van Breedam, J., van de Wal, R. S. W., Winkelmann, R., Zhao, C., Zhang, T., and Zwinger, T.: ISMIP6 Antarctica: a multi-model ensemble of the Antarctic ice sheet evolution over the 21st century, The Cryosphere, 14, 3033–3070, https://doi.org/10.5194/tc-14-3033-2020, publisher: Copernicus GmbH, 2020.

Shapiro, N. M. and Ritzwoller, M. H.: Inferring surface heat flux distributions guided by a global seismic model: particular application to Antarctica, Earth and Planetary Science Letters, 223, 213–224, https://doi.org/10.1016/j.epsl.2004.04.011, 2004.

535   Shepherd, A., Ivins, E., Rignot, E., Smith, B., van den Broeke, M., Velicogna, I., Whitehouse, P., Briggs, K., Joughin, I., Krinner, G.,
Nowicki, S., Payne, T., Scambos, T., Schlegel, N., A, G., Agosta, C., Ahlstrøm, A., Babonis, G., Barletta, V., Blazquez, A., Bonin, J.,
Csatho, B., Cullather, R., Felikson, D., Fettweis, X., Forsberg, R., Gallee, H., Gardner, A., Gilbert, L., Groh, A., Gunter, B., Hanna, E.,
Harig, C., Helm, V., Horvath, A., Horwath, M., Khan, S., Kjeldsen, K. K., Konrad, H., Langen, P., Lecavalier, B., Loomis, B., Luthcke, S.,
McMillan, M., Melini, D., Mernild, S., Mohajerani, Y., Moore, P., Mouginot, J., Moyano, G., Muir, A., Nagler, T., Nield, G., Nilsson, J.,
540   Noel, B., Otosaka, I., Pattle, M. E., Peltier, W. R., Pie, N., Rietbroek, R., Rott, H., Sandberg-Sørensen, L., Sasgen, I., Save, H., Scheuchl,
B., Schrama, E., Schröder, L., Seo, K.-W., Simonsen, S., Slater, T., Spada, G., Sutterley, T., Talpe, M., Tarasov, L., van de Berg, W. J.,
van der Wal, W., van Wessem, M., Vishwakarma, B. D., Wiese, D., Wouters, B., and The IMBIE team: Mass balance of the Antarctic Ice
Sheet from 1992 to 2017, Nature, 558, 219–222, https://doi.org/10.1038/s41586-018-0179-y, number: 7709 Publisher: Nature Publishing
Group, 2018.

545   Souverijns, N., Gossart, A., Demuzere, M., Lenaerts, J., Medley, B., Gorodetskaya, I., Vanden Broucke, S., and van Lipzig, N.:
Atmospheric climate model output of the COSMO-CLM2 regional climate model hindcast run over Antarctica (1987-2016),
https://doi.org/10.5281/zenodo.2539147, 2019.

Sutter, J., Fischer, H., Grosfeld, K., Karlsson, N. B., Kleiner, T., Van Liefferinge, B., and Eisen, O.: Modelling the Antarctic Ice Sheet across
the mid-Pleistocene transition – implications for Oldest Ice, The Cryosphere, 13, 2023–2041, https://doi.org/10.5194/tc-13-2023-2019,
550   publisher: Copernicus GmbH, 2019.

Sutter, J., Fischer, H., and Eisen, O.: Investigating the internal structure of the Antarctic ice sheet: the utility of isochrones for spatiotemporal
ice-sheet model calibration, The Cryosphere, 15, 3839–3860, https://doi.org/10.5194/tc-15-3839-2021, publisher: Copernicus GmbH,
2021.

van Dalum, C. T., van de Berg, W. J., and van den Broeke, M. R.: Impact of radiation penetration on Antarctic surface melt and subsurface
555   snow temperatures in RACMO2.3p3, preprint, Ice sheets/Antarctic, https://doi.org/10.5194/tc-2021-298, 2021.

van de Berg, W. J. and Medley, B.: Brief Communication: Upper-air relaxation in RACMO2 significantly improves modelled interannual sur-
face mass balance variability in Antarctica, The Cryosphere, 10, 459–463, https://doi.org/10.5194/tc-10-459-2016, publisher: Copernicus
GmbH, 2016.

van Wessem, J. M., van de Berg, W. J., Noël, B. P. Y., van Meijgaard, E., Amory, C., Birnbaum, G., Jakobs, C. L., Krüger, K., Lenaerts, J.
560   T. M., Lhermitte, S., Ligtenberg, S. R. M., Medley, B., Reijmer, C. H., van Tricht, K., Trusel, L. D., van Ulft, L. H., Wouters, B., Wuite,
J., and van den Broeke, M. R.: Modelling the climate and surface mass balance of polar ice sheets using RACMO2 – Part 2: Antarctica
(1979–2016), The Cryosphere, 12, 1479–1498, https://doi.org/10.5194/tc-12-1479-2018, publisher: Copernicus GmbH, 2018.

WCRP Global Sea Level Budget Group: Global sea-level budget 1993–present, Earth System Science Data, 10, 1551–1590,
https://doi.org/10.5194/essd-10-1551-2018, publisher: Copernicus GmbH, 2018.

565   Winkelmann, R., Martin, M. A., Haseloff, M., Albrecht, T., Bueler, E., Khroulev, C., and Levermann, A.: The Potsdam Parallel Ice Sheet
Model (PISM-PIK) – Part 1: Model description, The Cryosphere, 5, 715–726, https://doi.org/10.5194/tc-5-715-2011, publisher: Coperni-
cus GmbH, 2011.